



Calhoun: The NPS Institutional Archive DSpace Repository

Theses and Dissertations

1. Thesis and Dissertation Collection, all items

2002-12

Active mirror alignment for free electron lasers

Fiorani, Fulvia M.

Monterey, Calif. Naval Postgraduate School

<http://hdl.handle.net/10945/3981>

This publication is a work of the U.S. Government as defined in Title 17, United States Code, Section 101. Copyright protection is not available for this work in the United States.

Downloaded from NPS Archive: Calhoun



<http://www.nps.edu/library>

Calhoun is the Naval Postgraduate School's public access digital repository for research materials and institutional publications created by the NPS community.

Calhoun is named for Professor of Mathematics Guy K. Calhoun, NPS's first appointed -- and published -- scholarly author.

**Dudley Knox Library / Naval Postgraduate School
411 Dyer Road / 1 University Circle
Monterey, California USA 93943**

NAVAL POSTGRADUATE SCHOOL

Monterey, California



THESIS

ACTIVE MIRROR ALIGNMENT FOR FREE ELECTRON LASERS

by

Fulvia M. Fiorani

December 2002

Thesis Advisor:
Second Reader:

Bruce C. Denardo
Thomas J. Hofler

Approved for public release; distribution is unlimited

THIS PAGE INTENTIONALLY LEFT BLANK

REPORT DOCUMENTATION PAGE			Form Approved 0704-0188	OMB No. 0704-0188
<p>Public reporting burden for this collection of information is estimated to average 1 hour per response, including the time for reviewing instruction, searching existing data sources, gathering and maintaining the data needed, and completing and reviewing the collection of information. Send comments regarding this burden estimate or any other aspect of this collection of information, including suggestions for reducing this burden, to Washington Headquarters Services, Directorate for Information Operations and Reports, 1215 Jefferson Davis Highway, Suite 1204, Arlington, VA 22202-4302, and to the Office of Management and Budget, Paperwork Reduction Project (0704-0188) Washington DC 20503.</p>				
1. AGENCY USE ONLY (Leave blank)	2. REPORT DATE	3. REPORT TYPE AND DATES COVERED		
	December 2002	Master's Thesis		
4. TITLE AND SUBTITLE: Active Mirror Alignment for Free Electron Lasers			5. FUNDING NUMBERS	
6. AUTHOR Fiorani, Fulvia M.			8. PERFORMING ORGANIZATION REPORT NUMBER	
7. PERFORMING ORGANIZATION NAME(S) AND ADDRESS(ES) Naval Postgraduate School Monterey, CA 93943-5000				
9. SPONSORING / MONITORING AGENCY NAME(S) AND ADDRESS(ES) N/A			10. SPONSORING / MONITORING AGENCY REPORT NUMBER	
11. SUPPLEMENTARY NOTES The views expressed in this thesis are those of the author and do not reflect the official policy or position of the Department of Defense or the U.S. Government.				
12a. DISTRIBUTION / AVAILABILITY STATEMENT Approved for public release; distribution is unlimited.			12b. DISTRIBUTION CODE	
<p>ABSTRACT (maximum 200 words) This thesis investigates active mirror alignment systems of a free electron laser (FEL) for future integration as a ship self-defense weapon. An issue with this integration is the effect of low-frequency shipboard vibrations on the optical cavity mirrors. Alignment of the cavity mirrors is required for the proper operation of any type of laser. Mirror alignment is especially critical for an FEL because the electron beam and optical mode must substantially overlap. Laboratory FEL facilities, along with other laboratory high energy facilities that employ active mirror alignment systems, are investigated. In addition, a model theory for controlling the vibrations of a single-degree-of-freedom system is developed, and experiments with a simple mirror alignment system are described. Reduction of an impressed vibration amplitude by a factor of five is achieved, compared to a factor of fifteen that is achieved in major laboratory systems with sophisticated control systems. The purpose of these efforts is to understand the underlying physics of vibration control. The knowledge forms a basis for follow-on research towards the development of a prototype shipboard active mirror alignment system.</p>				
14. SUBJECT TERMS Free-Electron Lasers, Directed Energy Weapons, Active Control, Vibration Stabilization			15. NUMBER OF PAGES	83
16. PRICE CODE				
17. SECURITY CLASSIFICATION OF REPORT Unclassified	18. SECURITY CLASSIFICATION OF THIS PAGE Unclassified	19. SECURITY CLASSIFICATION OF ABSTRACT Unclassified	20. LIMITATION OF ABSTRACT UL	

NSN 7540-01-280-5500

Standard Form 298 (Rev. 2-89)
Prescribed by ANSI Std. Z39-18

THIS PAGE INTENTIONALLY LEFT BLANK

Approved for public release; distribution is unlimited

**ACTIVE MIRROR ALIGNMENT FOR
FREE ELECTRON LASERS**

Fulvia M. Fiorani
Lieutenant Commander, United States Navy
B.S., Embry-Riddle Aeronautical University (ERAU), 1991
Master of Aeronautical Science, ERAU, 2000

Submitted in partial fulfillment of the
requirements for the degree of

MASTER OF SCIENCE IN APPLIED PHYSICS

from the

**NAVAL POSTGRADUATE SCHOOL
December 2002**

Author: Fulvia M. Fiorani

Approved by: Bruce C. Denardo
Thesis Advisor

Thomas J. Hofler
Second Reader

William B. Maier II
Chairman, Department of Physics

THIS PAGE INTENTIONALLY LEFT BLANK

ABSTRACT

This thesis investigates active mirror alignment systems of a free electron laser (FEL) for future integration as a ship self-defense weapon. An issue with this integration is the effect of low-frequency shipboard vibrations on the optical cavity mirrors. Alignment of the cavity mirrors is required for the proper operation of any type of laser. Mirror alignment is especially critical for an FEL because the electron beam and optical mode must substantially overlap. Laboratory FEL facilities, along with other laboratory high energy facilities that employ active mirror alignment systems, are investigated. In addition, a model theory for controlling the vibrations of a single-degree-of-freedom system is developed, and experiments with a simple mirror alignment system are described. Reduction of an impressed vibration amplitude by a factor of five is achieved, compared to a factor of fifteen that is achieved in major laboratory systems with sophisticated control systems. The purpose of these efforts is to understand the underlying physics of vibration control. The knowledge forms a basis for follow-on research towards the development of a prototype shipboard active mirror alignment system.

THIS PAGE INTENTIONALLY LEFT BLANK

TABLE OF CONTENTS

I. INTRODUCTION.....	1
A. FREE-ELECTRON LASERS AS SHIP SELF-DEFENSE WEAPONS	1
B. THESIS OBJECTIVES	3
II. FEL PRINCIPLES OF OPERATION.....	5
III. OPTICAL CAVITY STABILITY REQUIREMENTS FOR A 1 MW FREE ELECTRON LASER.....	11
A. FEL EFFICIENCY REQUIRED TO DESTROY AN INCOMING MISSILE	11
B. MIRROR ANGULAR TOLERANCE.....	13
IV. FACILITIES WITH ACTIVE MIRROR ALIGNMENT SYSTEMS.....	19
A. DUKE FEL LABORATORY (OK-4/DUKE FEL)	19
B. JEFFERSON LAB (10 KW FEL).....	21
C. ADVANCED LIGHT SOURCE (ALS).....	24
D. KEK PARTICLE ACCELERATOR.....	26
E. AIRBORNE LASER (ABL).....	27
F. BOEING VISIBLE FEL FACILITY	28
V. CONTROL THEORY	29
A. MODEL SYSTEM	29
B. STABILITY	32
C. CONTROL OF STEADY-STATE VIBRATIONS	33
D. CONTROL OF TRANSIENT VIBRATIONS	35
VI. ACTIVE MIRROR ALIGNMENT EXPERIMENT	39
A. BASIC DESIGN AND COMPONENTS.....	39
1. Position Sensing Detector	40
2. Actuator System	41
3. Reference Laser	42
4. Control Circuit.....	42

B. RESULTS.....	45
1. Proportional Control.....	45
2. Mirror Mount Characterization	49
3. Proportional-Derivative Control.....	52
VII. CONCLUSIONS AND FUTURE WORK	55
A. CONCLUSIONS	55
B. FUTURE WORK.....	56
LIST OF REFERENCES.....	57
BIBLIOGRAPHY	61
INITIAL DISTRIBUTION LIST	63

LIST OF FIGURES

Figure 1.	Basic FEL Configuration.....	6
Figure 2.	Model of a Stable Two-Mirror Resonator.....	13
Figure 3.	Symmetric Two-Mirror Resonator.....	15
Figure 4.	Optical Mode Translation.....	16
Figure 5.	OK-4/Duke FEL Mirror Control and Stabilization System	20
Figure 6.	Block Diagram of JLab's Active Alignment System	22
Figure 7.	Reference Laser and PSD Setup in the 10 KW FEL Optical Cavity	23
Figure 8.	Experimental Setup of the 32 m Reference Laser Path Length for the 10 KW FEL	23
Figure 9.	Active Mirror Feedback System for the IR Beamline 1.4 Complex	25
Figure 10.	Block Diagram of the One-Dimensional Alignment System at KEK	26
Figure 11.	Model System with a Single Degree of Freedom	30
Figure 12.	Model System Steady-State Response	34
Figure 13.	Response Curves of a Damped Driven Oscillator	37
Figure 14.	Block Diagram of the Experimental Alignment System.....	39
Figure 15.	Quad Photodiode Block Diagram	41
Figure 16.	Schematic of Quad Photodiode Control Box	43
Figure 17.	Proportional-Derivative Control Circuit Diagram.....	44
Figure 18.	Schematic of System Response with Initial Control Circuit	47
Figure 19.	System Response with Second Control Circuit	48

Figure 20.	Mirror Mount (driven piezo) Characterization	50
Figure 21.	Mirror Mount (controlled piezo) Characterization.....	51
Figure 22.	System Response with Proportional-Derivative Control	53

LIST OF TABLES

Table 1. Experimental Alignment System Components 40

Table 2. System Instability as a Function of Frequency 49

THIS PAGE INTENTIONALLY LEFT BLANK

LIST OF SYMBOLS

α	displacement gain (model system)
α_e	extinction coefficient due to aerosols at sea level
β	velocity gain (model system)
$\langle B \rangle$	average magnetic field of undulator
c	speed of light in vacuum
c_d	damping coefficient (model system)
E	energy of electron beam
F_o	constant force amplitude (model system)
$F(t)$	external force (model system)
φ	optical axis angular tilt
$G(t)$	force due to actuator (model system)
Γ	effective damping parameter (model system)
γ	damping parameter (model system)
γ_z	relativistic Lorentz factor
g_k	resonator parameter, $k = 1, 2$
I_k	quadrant photodiode output current, $k = 1, 2, 3, 4$
\bar{I}	average current of electron beam
\hat{I}	peak current of electron beam
K	undulator parameter
K_E	effective stiffness (model system)
k	spring constant (model system)
k_{em}	electromagnetic wave wavenumber
k_w	wiggler wavenumber
λ	wavelength of emitted radiation
λ_w	wiggler wavelength (or wiggler period)
L	wiggler length

m	total mass (model system)
m_0	electron rest mass
η	FEL efficiency
P_{beam}	power of electron beam
P_m	power required to destroy missile
P_{ship}	power required to leave ship
R	mirror radius of curvature
S	optical cavity length
V	electron beam voltage
V_k	quadrant photodiode output voltages, $k = 1, 2, 3, 4$
v_z	velocity of electron beam in z – direction
Ω	effective natural frequency (model system)
Ω_d	damped angular frequency (model system)
θ	mirror angular tilt
t	time
ω	drive frequency (model system)
ω_e	radial frequency of emitted radiation
ω_{em}	angular frequency of electromagnetic wave
ω_o	natural frequency (model system)
ω_q	oscillation frequency of electrons
ω'	electron oscillation frequency in moving reference frame
W_k	beam spot radius at cavity mirror, $k = 1, 2$
W_0	optical mode waist radius
x	mass displacement (model system)
Δy	optical mode displacement
Z_0	Rayleigh length
Z_k	distance from beam waist, $k = 1, 2$

LIST OF ACRONYMS

ALS	Advanced Light Source
COIL	Chemical Oxygen-Iodine Laser
CPU	Central Processing Unit
DAC	Digital-to-Analog Converter
FEL	Free-Electron Laser
GeV	Giga electron-volt
IR	Infrared
JLAB	Thomas Jefferson Accelerator Facility
KEK	High Energy Accelerator Research Organization (Japan)
KW	Kilowatt
MeV	Mega electron-volt
MW	Megawatt
OCMMS	Optical Cavity Mirror Metrology System
OK-4	Optical Klystron
PD	Proportional-Derivative Control
PID	Proportional, Integral, Derivative Control
PSD	Position Sensing Photodiode
PZT	Piezoelectric actuator (Plumbum Zirconate Titanate)
rms	root mean square
SLR	Single Lens Reflex
UV	Ultra Violet
VEPP-3	Vstrechnye Electron – Positron Puchke
XUV	extreme Ultra Violet

THIS PAGE INTENTIONALLY LEFT BLANK

ACKNOWLEDGMENTS

First, I would like to express my sincere appreciation to Professor Bruce Denardo, not only for his expert guidance and invaluable assistance with this thesis, but for the ever-present encouragement he gave throughout my two years at Naval Postgraduate School. Thank you.

I would also like to thank Professor Tom Hofler for his acoustics and electronics advice, and Sam Barone for his technical assistance. Thanks also to Dr. Michelle Shinn, Joe Gubeli and Chris Behre from Jefferson Laboratory who invited me to visit the 10 KW FEL upgrade facility and took time to show me around and explain their active mirror alignment system.

Finally, I thank my husband, John Springer, for his never-ending love, support and understanding throughout this endeavor, and always.

THIS PAGE INTENTIONALLY LEFT BLANK

I. INTRODUCTION

With the end of the Cold War, the United States Navy has defined a new strategic concept intended to carry the Naval Service into the 21st century. The Navy's post-Cold War strategic concept was first outlined in a 1992 Department of the Navy publication ...*From the Sea* [Department of the Navy] which announced a landmark shift in operational focus. This fundamental shift was a direct result of the changing strategic landscape – away from dealing with a global maritime threat and toward projecting power and influence across the seas in response to regional challenges.

The recent Naval mission shift from “blue water” to littoral conflict has had a great effect on cruise missile defense requirements. Instead of support defense within a battle group where crossing target engagements predominate, each ship must be capable of performing self-defense against an incoming threat. Existing low radar-cross-section, transonic, sea-skimming cruise missiles have already reduced the battle space towards the limits of current gun and missile defensive weapon systems. Meanwhile more capable supersonic and high-g maneuvering missiles are increasingly available [Todd, 1997].

Maritime forces in the twenty-first century will confront a formidable array of threats. Even without the emergence of a significant competitor, the U.S. Navy will face unprecedented challenges from the proliferation of sophisticated missile and sensor technology [McCarthy].

The development of advanced cruise missiles poses an economical and widely available weapon for most opponents that seek to attack any major naval power. The U.S. Navy must therefore develop new defensive systems and new approaches to battle group operations.

A. FREE-ELECTRON LASERS AS SHIP SELF-DEFENSE WEAPONS

Cruise missiles with increasingly sophisticated capability represent a very significant threat to present and future U.S. Naval operations. Today's naval

combatants face an increasingly difficult challenge of defending against state-of-the-art anti-ship missiles. These threats travel at high velocities with pin point accuracy and require a defensive system capable of both stopping an incoming missile while preventing debris damage to the warship.

As a result of the shift in operational emphasis from sea control to the influence of events in regional areas, Navy warships can be expected to operate in littoral regions of enemy territories, with an increased potential of encountering hostile forces. Even with the advanced defensive systems on board most naval combatants, the decreased reaction times available in littoral operations make them considerably more vulnerable to anti-ship cruise missiles. It is to defend against such threats, that directed energy weapons, specifically the free-electron laser (FEL), has been proposed as a future shipboard self-defense weapon system.

The theoretical advantage of an FEL as a high-power laser centers on the fact that it lases in a vacuum and the unconverted drive energy is carried away by the electrons at nearly the speed of light. This contrasts with conventional lasers where thermal constraints in the material lasing medium eventually lead to a power limit. A second advantage is the broad-band tunability of the FEL which can be achieved by varying the electron energy or the wiggler magnetic field. Since the wavelength is not dependent on particular atomic transitions lines as a conventional high-power laser, the FEL can be designed for operation at any wavelength [Todd, 1997].

As a ship self-defense weapon, an FEL provides a near instantaneous response to missile threats using a weapon traveling at the speed of light. Additionally, because of its improved response time, an FEL can engage incoming missiles at greater distances providing enhanced self-defense capability. Chapter II describes the basic principles of operation of a free-electron laser.

B. THESIS OBJECTIVES

To implement a functional FEL weapon system successfully into a Navy ship, many issues involving the integration of the FEL requirements and shipboard environment must be resolved. These include prime power availability, energy storage mechanisms, cryogen storage, radiation shielding, safety and control [Todd, 2001]. Another major issue, and the focus of this thesis, is the effect of low frequency vibrations on the optical cavity mirrors of the FEL. Proper alignment of the lasing medium (electron beam) and the optical beam are critical for FEL performance.

The objective of this thesis is to investigate FEL laboratory facilities that currently employ active optical cavity alignment systems (Chapter IV) and set up an experimental alignment system to understand the underlying physics of control theory. The knowledge gained from the experimental system will be used in follow-on research leading towards the development of a prototype shipboard alignment system. The experimental alignment system is described in Chapter VI.

THIS PAGE INTENTIONALLY LEFT BLANK

II. FEL PRINCIPLES OF OPERATION

In its fundamental concept, the free-electron laser is an extremely adaptable light source which can produce high-power coherent radiation across virtually the entire electromagnetic spectrum. Theoretical calculations indicate that free-electron lasers are capable of efficiencies as high as 65% while efficiencies of 40% have been demonstrated in the laboratory [Freund and Antonsen].

In a free-electron laser, high-energy electrons emit coherent radiation, as in a conventional laser, but the electrons travel in a beam through a vacuum instead of remaining in bound atomic states within the lasing medium. Because the electrons are free streaming, the radiation wavelength is not constrained by a particular transition between two discrete energy levels. In quantum mechanical terms, the electrons radiate by transitions between energy levels in the continuum and, therefore, radiation is possible over a much larger range of frequencies than is found in a conventional laser.

Reduced to its essentials, a free-electron laser consists of an accelerator to produce the electron beam, a “wiggler” to force the electrons to oscillate and therefore radiate, and an optical system to form the laser beam. These are shown schematically in Figure 1. As shown there, the wiggler consists of a series of dipole magnets of opposite polarity producing a linearly polarized transverse magnetic field which forces the electrons to move along sinusoidal trajectories. Helical wigglers are alternatively employed.

The radiation is produced by an interaction among three elements: (1) the relativistic electron beam; (2) an electromagnetic wave traveling in the same direction as the electrons; and (3) an undulatory magnetic field produced by the assembly of magnets. The wiggler magnetic field acts on the electrons in such a way that they acquire an undulatory motion. The acceleration associated with the electrons’ curvilinear trajectories generates radiation. In the process, the electrons lose energy to the electromagnetic wave which is amplified and emitted by the laser. The tunability of the free-electron laser arises because the

wavelength of light required for the interaction between these three elements is determined by both the periodicity of the wiggler field and the energy of the electron beam.

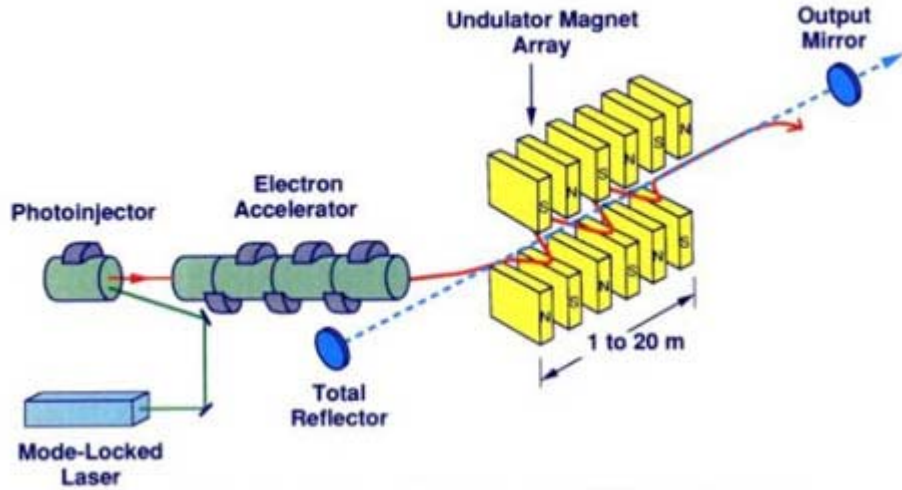


Figure 1. Basic FEL Schematic [from University of Maryland]

A uniform electron beam which traverses an undulatory magnetic field emits incoherent radiation. In order to give rise to stimulated emission required for a free-electron laser, it is necessary for the electron beam to form coherent bunches. This can occur when a light wave traverses an undulatory magnetic field such as the wiggler because the spatial variations of the wiggler and the electromagnetic wave combine to produce a beat wave, which is essentially an interference pattern [Freund and Antonsen]. It is the interaction between the electrons and this beat wave which gives rise to the stimulated emission in free-electron lasers.

The beat wave has the same frequency as the light wave, but its wavenumber is the sum of the wavenumbers of the electromagnetic and wiggler fields. With the same frequency, but larger wavenumber, the beat wave travels more slowly than the light wave, and is called the *ponderomotive* wave. Electrons moving in synchronism with the wave are said to be in resonance with it and will

experience a constant field. In such cases, the interaction between the electrons and the ponderomotive wave can be extremely strong. It is the ponderomotive force that causes electrons to speed up and slow down, therefore causing the electrons to bunch together.

The frequency of the electromagnetic wave required for this resonant interaction can be determined by matching the velocities of the ponderomotive wave and the electron beam. This is referred to as the *phase-matching condition*. The interaction is one in which an electromagnetic wave characterized by an angular frequency ω_{em} and wavenumber k_{em} and the magnetostatic wiggler with a wavenumber k_w produce a beat wave with the same frequency as the electromagnetic wave but a wavenumber equal to the sum of the wavenumbers of the wiggler and the electromagnetic waves ($k_{em} + k_w$). The velocity of the ponderomotive wave is given by the ratio of the frequency of the wave to its wavenumber. As a result, matching this velocity to that of the electron beam gives the resonance condition in a free-electron laser

$$\frac{\omega_{em}}{k_{em} + k_w} \cong v_z \quad (1)$$

for a beam with a bulk streaming velocity v_z in the z -direction (the z -direction indicates both the bulk streaming velocity of the electron beam and the symmetry axis of the wiggler field).

The dispersion relation between the frequency and wavenumber for waves propagating in free space is $\omega \approx ck$, where c denotes the speed of light in a vacuum. Combination of the free-space dispersion relation and the free-electron laser resonance condition (1) gives the standard relation for the wavelength as function of both the electron beam energy and the wiggler period

$$\lambda \cong \frac{\lambda_w}{2\gamma_z^2} \quad (2)$$

where $\gamma_z = (1 - v_z^2/c^2)^{-1/2}$ is the relativistic Lorentz factor which is related to the electron streaming energy, and $\lambda_w = 2\pi/k_w$ is the wiggler wavelength. The approximation $v_z \approx c$ is made in the derivation of Eq. (2). The wavelength is directly proportional to the wiggler period and inversely proportional to the square of the streaming energy. This results in a broad tunability which permits the free-electron laser to operate across virtually the entire electromagnetic spectrum. By using different types of accelerators to produce electrons of different energies, it is possible to obtain wavelengths from the microwave region to the ultraviolet.

To better understand how the interaction between the three elements occurs, we consider the case of spontaneously emitted radiation, i.e. when no mirrors are used [Svelto, O.]. Once injected in the periodic structure, the electrons acquire an undulatory motion in the plane orthogonal to the magnetic field. The resulting electron acceleration produces a longitudinal emission of the synchrotron type. The frequency of the emitted radiation can be derived by noting that the electron oscillates in the transverse direction at an angular frequency

$$\omega_q = \left(\frac{2\pi}{\lambda_w} \right) v_z \approx \left(\frac{2\pi}{\lambda_w} \right) c, \quad (3)$$

where λ_w is the wavelength of the wiggler, also called the magnet period, and v_z is the (average) longitudinal velocity of the electron (which is almost equal to the vacuum light velocity c). Now we consider a reference frame moving longitudinally at velocity v_z . In this frame, the electron oscillates essentially in the transverse direction; thus it looks like an oscillating electric dipole. In this reference frame, due to the Lorentz time contraction, the oscillation frequency is given by

$$\omega' = \frac{\omega_q}{\left[1 - (v_z/c)^2\right]^{1/2}} \quad (4)$$

and is therefore the frequency of the emitted radiation in the moving reference frame. If we now go back to the laboratory frame, the radiation frequency undergoes a (relativistic) Doppler shift. The observer radial frequency ω_e and the corresponding wavelength λ are then given by

$$\omega_e = \frac{1 + (v_z/c)}{\left[1 - (v_z/c)^2\right]^{1/2}} \omega' \equiv \frac{2\omega_q}{1 - (v_z/c)^2} \quad (5)$$

and substituting Eq. (3) into Eq. (5),

$$\lambda = \frac{\lambda_w}{2} \left[1 - (v_z/c)^2\right]. \quad (6)$$

This is identical to Eq. (2), which was derived from a different perspective. Note that, since $v_z \approx c$, λ is generally much smaller than the magnet period. To calculate the quantity $\gamma^{-2} = 1 - (v_z/c)^2$ in Eqs. (5) and (6), we recall from special relativity that for a free electron moving with velocity v_z along the z -axis, we have $E = \gamma mc^2$, or

$$1 - \left(\frac{v_z}{c}\right)^2 = \left(\frac{m_0 c^2}{E}\right)^2, \quad (7)$$

where m_0 is the rest mass of the electron and E its energy. However, for a given total energy, the wiggling motion reduces the value of v_z , therefore it

increases the value of $\left[1 - (v_z/c)^2\right]$. A detailed calculation, (not shown here) then shows that this quantity is given by

$$1 - (v_z/c)^2 = (1 + K^2) \left(\frac{m_0 c^2}{E} \right)^2 \quad (8)$$

where K is a numerical constant and is called the *undulator parameter*. Its value is obtained from the expression $K = e \langle B^2 \rangle^{1/2} \lambda_w / 2\pi m_e c^2$, where B is the magnetic field of the undulator and the average is taken along the longitudinal direction. Substituting Eq. (8) into Eqs. (5) and (6), we obtain

$$\omega_e = \frac{4\pi c}{\lambda_w} \left(\frac{1}{1 + K^2} \right) \left(\frac{E}{m_0 c^2} \right)^2 \quad (9)$$

and

$$\lambda = \frac{\lambda_w}{2} \left(\frac{m_0 c^2}{E} \right)^2 (1 + K^2) \quad (10)$$

which shows that the wavelength of the emitted radiation can be changed by either changing the magnet period λ_w , the energy E of the electron beam and/or the magnetic field (embedded in the undulator parameter K .)

III. OPTICAL CAVITY STABILITY REQUIREMENTS FOR A 1 MW FREE ELECTRON LASER

A one-megawatt (1 MW) FEL has been proposed as a shipboard self-defense weapon system. Such a high power FEL, however, leads to high intensity on the optical cavity mirrors and may cause damage. To avoid this, the spot intensity must be reduced to within mirror tolerance. One way to accomplish this is to increase the spot size on the mirrors by decreasing the Rayleigh length. This is the characteristic distance for laser beam diffraction and describes the distance for the spot radius to double in size from a flat phase front.

By decreasing the Rayleigh length, the spot on the mirror increases and the intensity decreases. However, decreasing the Rayleigh length also affects the stability and efficiency of the FEL. In order to maintain stability and maximize efficiency, the optical cavity must display good mode control. With the increased optical mode spot size at the mirrors, cavity mirror misalignment may have a significant effect on the behavior of the cavity modes and therefore on the stability and efficiency of the FEL itself.

This chapter first estimates the efficiency required for a 1 MW shipboard FEL to destroy an incoming missile, and then establishes the minimum mirror angular tolerance that an active mirror alignment system would need to achieve in order to maintain such an efficiency.

A. FEL EFFICIENCY REQUIRED TO DESTROY AN INCOMING MISSILE

The FEL efficiency η needed to supply sufficient laser power to destroy an incoming missile is defined as the power required to leave the ship P_{ship} divided by the power of the electron beam P_{beam} ,

$$\eta = \frac{P_{ship}}{P_{beam}}. \quad (11)$$

To calculate P_{ship} , we first estimate the laser power P_m required to destroy the missile. The energy required is $8kW/cm^2$ on a spot of approximately $5cm$ radius for a 3 second duration [Colson, May 2002]. Hence,

$$P_m = \frac{8kW}{cm^2} (\pi r^2) = \frac{8kW}{cm^2} (125\pi) = 0.628 \text{ MW} . \quad (12)$$

Accounting for attenuation through the atmosphere as the beam propagates toward the target, the laser power required to leave the ship can be expressed as

$$P_{ship} = P_m e^{\alpha_e z} \quad (13)$$

where, α_e is the extinction coefficient due to aerosols at sea level ($\alpha_e = 0.02km^{-1}$), and z is the estimated distance to the missile ($z = 6km$). Substituting Eq. (12) into Eq. (13), we find

$$P_{ship} = 0.708 \text{ MW} . \quad (14)$$

The power of the electron beam is given by

$$P_{beam} = V\bar{I} \quad (15)$$

where $V = 185MV$ (from the electron beam energy, $KE = 185MeV$) and \bar{I} is the average current of the electron beam. The average current is expressed as $\bar{I} = \hat{I}D$, where $\hat{I} = 3.2kA$ is the peak current [Crooker], and D is a duty factor $D = W_0/L$, where $W_0 = 0.1mm$ is the optical waist of the beam and $L = 60cm$ is the length of the wiggler [Colson, 2001]. Substituting these values into Eq. (15), gives

$$P_{beam} = 98.7 \text{ MW} \quad (16)$$

Finally, substituting Eqs. (14) and (16) into Eq. (11), we estimate the 1 MW FEL efficiency required to destroy an incoming missile to be

$$\eta \approx 0.7\%. \quad (17)$$

B. MIRROR ANGULAR TOLERANCE

The optical cavity of an FEL is a stable two-mirror type resonator. In such a resonator, a set of lowest-order gaussian modes or beams can bounce back and forth between the two mirrors, thus trapping the gaussian beam as a standing wave. The physical properties of these beams and stable resonator modes are well known [Siegman], however, to better understand the effects of mirror misalignment in stable resonators, a brief summary of basic general properties is provided. Figure 2 shows a simple model for analyzing stable two-mirror cavities, where W_0 is the initial spot radius (gaussian beam waist), W_1 and W_2 are the spot radii at the ends of the resonator, Z_1 and Z_2 are the distances of the two mirrors relative to the gaussian beam waist at $Z = 0$, R_1 and R_2 are the radii of curvature of mirror 1 and mirror 2, respectively; and S is the length of the resonator.

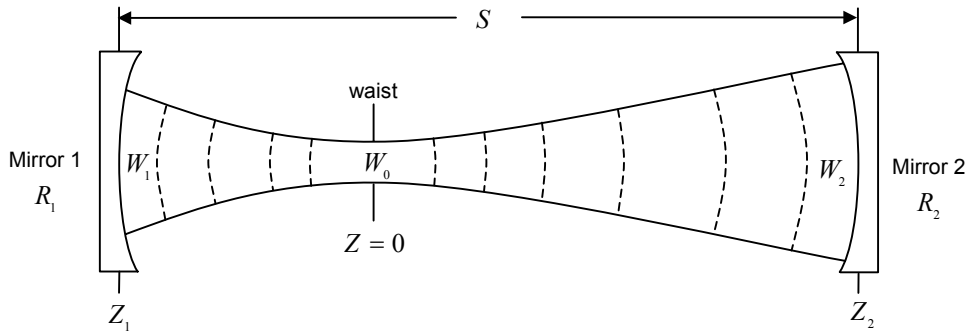


Figure 2. Model of a Stable Two-Mirror Resonator.

It is convenient to define resonator “g” parameters in terms of the resonator length and the mirror radius of curvature:

$$g_1 \equiv 1 - \frac{S}{R_1} \quad \text{and} \quad g_2 \equiv 1 - \frac{S}{R_2} . \quad (18)$$

In terms of these parameters [Siegman], the Rayleigh length is

$$Z_0^2 = \frac{g_1 g_2 (1 - g_1 g_2)}{(g_1 + g_2 - 2g_1 g_2)^2} S^2 , \quad (19)$$

the gaussian beam waist is

$$W_0^2 = \frac{S\lambda}{\pi} \sqrt{\frac{g_1 g_2 (1 - g_1 g_2)}{(g_1 + g_2 - 2g_1 g_2)^2}} , \quad (20)$$

and the spot radii at the ends of the resonator are

$$W_1 = \frac{S\lambda}{\pi} \sqrt{\frac{g_2}{g_1 (1 - g_1 g_2)}} \quad \text{and} \quad W_2 = \frac{S\lambda}{\pi} \sqrt{\frac{g_1}{g_2 (1 - g_1 g_2)}} . \quad (21)$$

From Eqs. (19) through (21), we see that real and finite solutions to beam parameters and spot sizes can only exist if $0 \leq g_1 g_2 \leq 1$. This condition defines the stability range of the resonator.

The FEL resonator is a symmetric, near-concentric ($R \approx S/2$) stable two-mirror type resonator (Figure 3), where $Z_1 = Z_2 = Z$, $W_1 = W_2 = W$, and $R_1 = R_2 = R$, hence $g_1 = g_2 = g = 1 - \frac{S}{R}$.

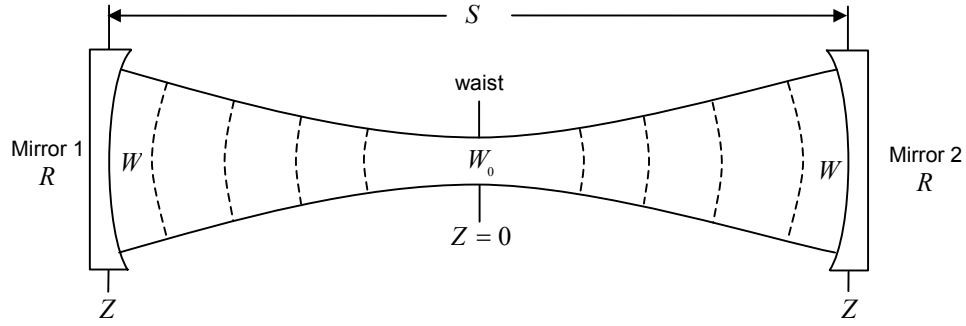


Figure 3. Symmetric Two-Mirror Resonator.

Using these symmetry conditions, Eqs. (19) through (21) can be simplified as

$$Z_0 = \left[\frac{1+g}{4(1-g)} S^2 \right]^{1/2}, \quad (22)$$

$$W_0 = \left[\frac{S\lambda}{\pi} \sqrt{\frac{1+g}{4(1-g)}} \right]^{1/2}, \quad (23)$$

$$W = \left[\frac{S\lambda}{\pi} \sqrt{\frac{1}{1-g^2}} \right]^{1/2}. \quad (24)$$

Misalignment of either mirror in a stable two-mirror resonator causes a rotation of the optical axis. The optical axis is defined as the line passing through the centers of curvature of the two mirrors. Figure 4 is a schematic of the optical mode translation due to mirror tilt. The angles are greatly exaggerated and the

optical mode is shown with maximum translation while still overlapping the electron beam.

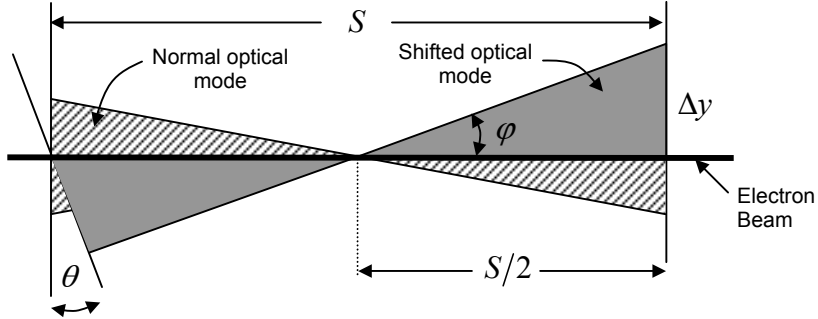


Figure 4. Optical Mode Translation (angles greatly exaggerated).

When one of the mirrors is tilted by an angle θ , the optical axis will be tilted by an angle φ resulting in an optical mode shift and an off-center translation Δy of the mode spot on the mirror. Using simple trigonometry, we can calculate how far the optical mode will be translated by a small angular rotation of the mirror. From Figure 4, we see that $\Delta y = \tan \varphi (S/2)$. Using the small angle approximation $\tan \varphi = \varphi$, the displacement of the mode translation is given by

$$\Delta y = \frac{S}{2} \varphi \quad , \quad (25)$$

where the angular displacement φ of the optical axis can be written in terms of the resonator parameter and the mirror tilt angle [Siegman]

$$\varphi = (1 + g) \theta . \quad (26)$$

For lasing to occur in a free-electron laser, the electron beam and the optical mode must overlap. Therefore, the optical mode must not be rotated outside of

the electron beam, or alternatively, the mode spot on the mirror must not translate more than the beam radius W . We can express this limiting condition as

$$\Delta y_{\max} = W. \quad (27)$$

Using the optical cavity parameters of the 1 MW FEL ($S=12m$, $Z_0=1.8cm$, and $g=1-\frac{S}{R}$, where $R=\frac{S}{2}+\frac{Z_0^2}{(S/2)}$) and substituting these values into Eq. (24), we determine the beam spot radius on the mirror to be $W=25mm$. This result is also equal to the maximum displacement of the optical mode (Δy_{\max}) from Eq. (27). Given the maximum displacement, we can now calculate the maximum angular displacement of the optical axis by substituting $\Delta y_{\max}=25mm$ into Eq. (25), which gives us $\varphi_{\max}=4.2mrad$. Finally, we can determine the maximum angular mirror tilt by substituting φ_{\max} into Eq. (26), which yields the maximum angular tolerance $\theta_{\max}=0.08\mu rad$.

It is important to note, however, that the above angular tolerance was derived geometrically for a no-gain (cold cavity) resonator. Results of FEL simulations conducted at the Naval Postgraduate School have shown that when cavity gain is present, the maximum allowable mirror angular tilt, while still maintaining the minimum required efficiency ($\eta=0.7\%$), increases to $\theta_{\max}=180\mu rad$ [Crooker]. These simulated results show that allowable mirror tilt (with cavity gain) is approximately 3 orders of magnitude greater than cold cavity theory predictions, suggesting that the electron beam plays a significant role in determining the actual optical mode translation.

Although laboratory FEL active mirror alignment systems have achieved stability to within $0.1\mu rad$ (see Duke FEL, Chapter IV), it is not yet known if such level of stability is achievable in a shipboard environment. However, based on simulations of the proposed 1 MW shipboard FEL, it appears that it would be

sufficient for a shipboard active alignment system to achieve mirror stability on the order of $\theta \approx 100 \mu\text{rad}$.

IV. FACILITIES WITH ACTIVE MIRROR ALIGNMENT SYSTEMS

Active stabilization of mirrors in optical systems is not a new concept. As optical technologies continue to advance, the need to achieve greater precision and resolution has pushed passive damping systems to their limits.

Active stabilization systems are used in fields such as astronomy (together with adaptive optics), high-energy physics (particle accelerators), and laboratory FEL facilities. However, active stabilization systems are not limited to large research facilities, but can be found in “everyday life” systems. Canon’s EOS-1V (AF 35mm SLR camera) has an active mirror control system to reduce mirror bounce and camera shake [Canon]. Additionally, many hand-held video cameras have optical stabilization systems.

This chapter briefly describes active mirror stabilization systems currently employed by two laboratory FEL facilities (Duke University and Jefferson Lab); the active feedback mirror system employed by Advanced Light Source (ALS) at Lawrence Berkeley National Laboratory; and the active alignment system at the High Energy Accelerator Research Organization (KEK) in Ibaraki, Japan. Additionally, the U.S. Air Force’s Airborne Laser and the Boeing Visible FEL Facility are briefly mentioned.

A. DUKE FEL LABORATORY (OK-4/Duke FEL)

Duke University operates two free-electron lasers at the Duke FEL Laboratory: the Mark III infrared FEL and the OK-4 (optical klystron)/storage ring FEL which produces UV and XUV laser beams as well as gamma rays via Compton scattering. The OK-4 FEL system was developed in collaboration with the Budker Institute of Nuclear Physics in Novosibirsk, Russia. The system utilizes Duke’s 1.1 GeV electron storage ring and the OK-4 undulator and optical system originally developed and commissioned at Budker for use on the VEPP-3 storage ring [Madey].

To reduce power density and damage to mirrors, the OK-4 FEL has a very long optical cavity (53.7 m) with a Rayleigh length of 3.3 m [Pinayev, 1999]. The significant mismatch between cavity length and Rayleigh range makes the OK-4 FEL very susceptible to mirror vibrations and misalignment. To stabilize the optical cavity, Duke employs passive damping methods to suppress high-frequency, while low-frequency vibrations and drift are suppressed by using an active stabilization system. The general layout of the mirror control and stabilization system for the OK-4 FEL [Pinayev, 1998] is shown in Figure 5.

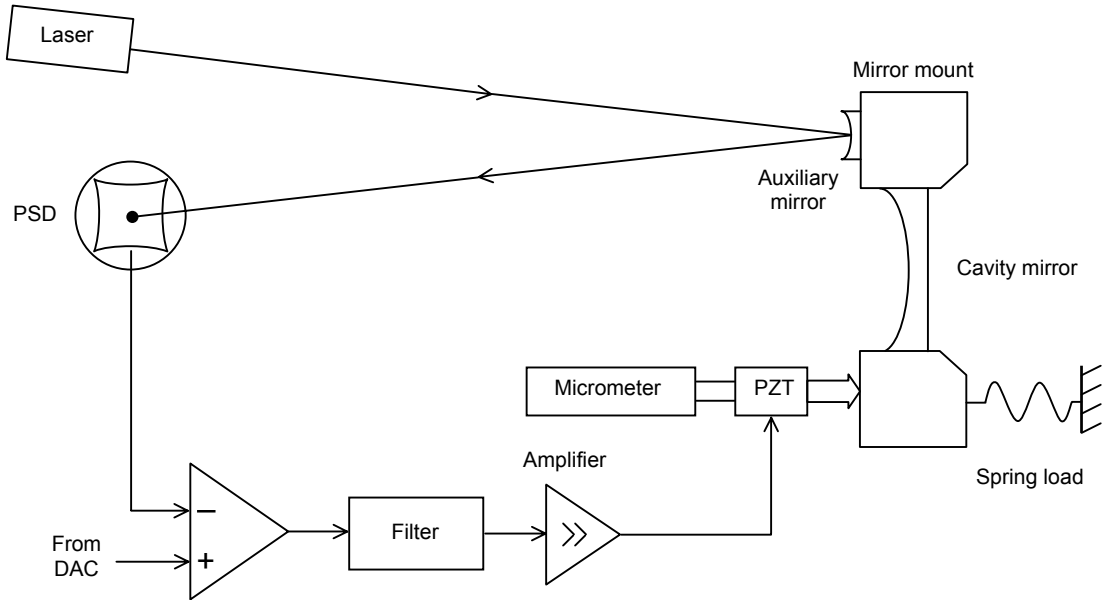


Figure 5. OK-4/Duke FEL Mirror Control and Stabilization System.
From [Pinayev, 1998]

The tilt angle of the cavity mirror mount is measured with the help of an auxiliary mirror firmly attached to the mirror mount. The cavity mirror mount is controlled by $30\text{ }\mu\text{m}$ P-830.20 piezotranslators manufactured by Polytec PI. Coarse mirror adjustment is done manually using micrometers, while fine adjustment of the mirrors is controlled by four 16-bit digital-to-analog converters (DAC). Light from a small semiconductor reference laser reflects from the auxiliary mirror onto a position sensing photodiode (PSD) S2044 manufactured

by Hamamatsu. The signal from the PSD is processed by a built-in analog circuit, which provides output voltages proportional to the displacement of the light spot from the center of the detector. The signal is then compared to the control voltage from the DAC and the error signal is amplified to change the voltage on the piezoelectric actuator (PZT).

Testing of Duke's prototype system revealed a much lower cut-off frequency than was estimated using the piezo stiffness and mirror mount inertia. They also found a strong mechanical resonance of the mirror mount around 100 Hz . A gain-phase filter was installed to provide a higher cut-off frequency with a substantial phase margin for stability. The installation of the filter raised the cut-off frequency from 1 Hz to 50 Hz . The correction filter also integrated the error signal, providing better long-term stability.

Implementation of the optical control system resulted in mirror vibrations below 100 *nanoradians* with negligible drift. For a more detailed description of this system, see Pinayev, "System for the Control and Stabilization of OK-4/Duke FEL Optical Cavity" [Pinayev, 1998].

A. JEFFERSON LAB (10 KW FEL)

Thomas Jefferson National Accelerator Facility (JLab) is currently in the process of upgrading its one-kilowatt (KW) infrared (IR) demonstration FEL to a 10 KW facility. The FEL upgrade will enable an operating wavelength range between 0.25 - 15 μm and an average power of up to 10 KW [JLab].

The optical cavity for the 10 KW FEL is a near concentric resonator design with a cavity length of 32.042 m , a Rayleigh length of 2 m and a mirror radius of curvature of 16.271 m . The length of the cavity and its near concentric design set more stringent requirements on the optical cavity mirror alignment tolerance.

To ensure the optical cavity exhibits good mode control in order to maximize FEL efficiency, JLab has developed an active alignment system called the Optical Cavity Mirror Metrology System (OCMMS) to actively stabilize the mirrors to within 1 $\mu radian$. The active stabilization system is designed to

stabilize mirrors due to ground vibrations for a bandwidth of 1 - 100 Hz [Shinn]. A block diagram of the system is shown in Figure 6.

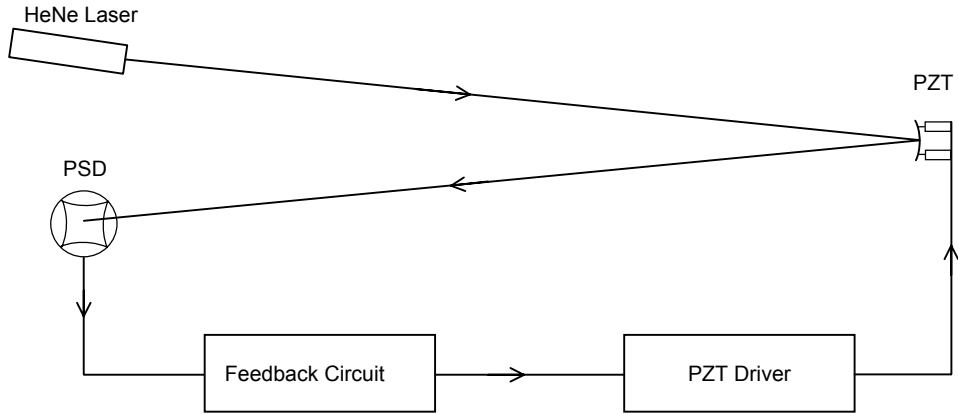


Figure 6. Block Diagram of JLab's Active Alignment System. From [Behre]

Similar to Duke's system, JLab utilizes a reference laser to sense the vibrations of the cavity mirror, but unlike Duke, the reference laser reflects from the cavity mirror, not an auxiliary mirror. Light is reflected from the mirror to a two-dimensional silicon position sensing photodiode (Hamamatsu, S1881 PSD with processing circuit C4674). The signal from the PSD is compared to a preset value, designating the desired position of the beam, in an analog feedback circuit. Any error from the comparison is then amplified and the signal sent to the piezoelectric actuators via the piezo driver (Piezosystem Jena ultra high vacuum compatible PA 16/12).

The actual path the reference laser will travel is approximately the distance from the center of the wiggler to the cavity mirror and back. Figure 7 shows the final design with the reference laser and PSD within the optical cavity. Although JLab has not yet installed the OCMMS on the 10 KW FEL Upgrade, an experimental system has been set up to duplicate the total path length (32m) the reference laser will travel. To achieve this distance experimentally, the path

length was folded several times on a 14-foot optical table. Figure 8 shows a diagram of the experimental setup.

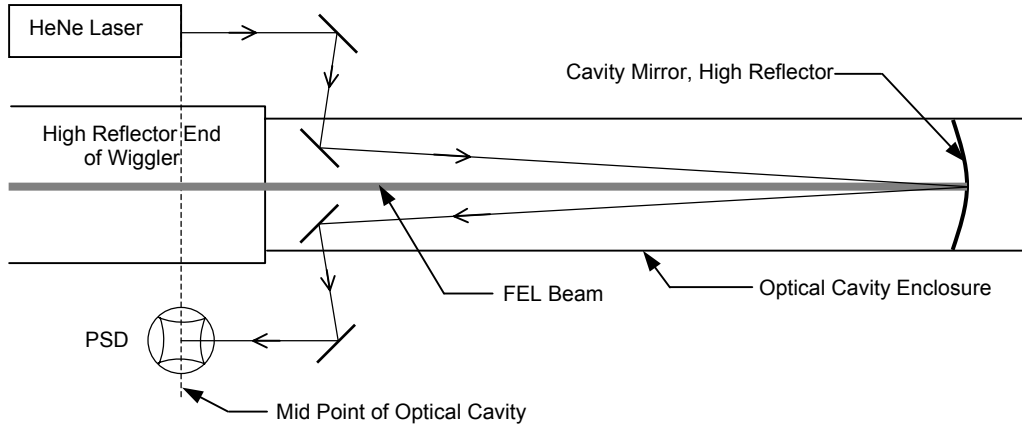


Figure 7. Reference Laser and PSD Setup in the 10 KW FEL Optical Cavity. From [Behre]

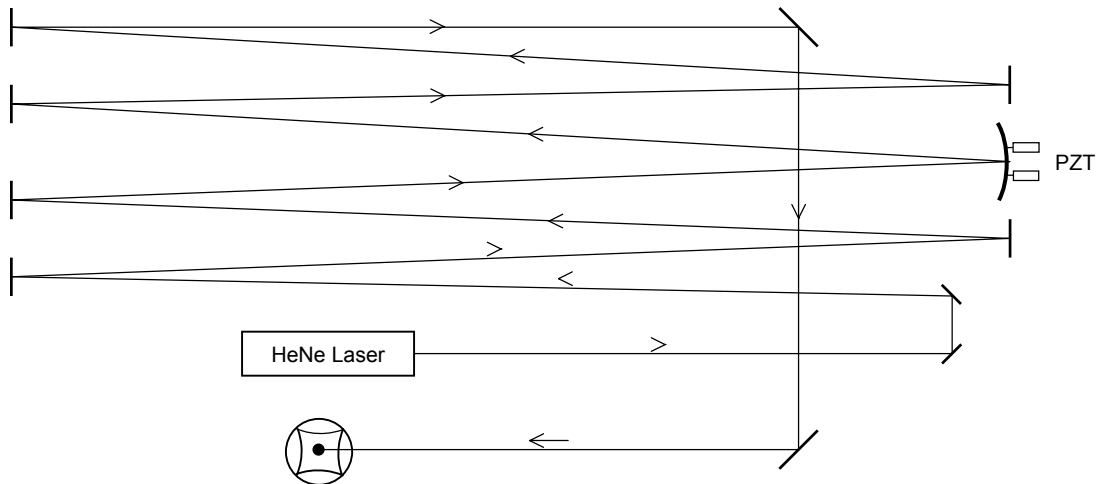


Figure 8. Experimental Setup of the 32m Reference Laser Path Length for the 10 KW FEL. From [Behre]

Preliminary testing and characterization of the experimental system found that the mechanical mirror mount had resonances at $\sim 50, 110$ and 150 Hz.

Various attempts were made to mechanically reduce the resonances of the mirror mount. These included adding mass, strengthening the support legs and replacing the springs with higher spring constant springs. Although these attempts slightly shifted the frequencies, they remained in the operating band. The next course of action was to filter the resonant frequencies electronically. A combination of a Chebyshev and Twin-T Notch filter was used. This setup allowed the experimental system to operate without noticeable resonance spikes.

As of this writing, a final design of the OCMMS was not available. For a more detailed description of JLab's experimental active mirror stabilization system, see Behre, *Optical Cavity Mirror Stabilization System* [Behre].

C. ADVANCED LIGHT SOURCE (ALS)

The Advanced Light Source is a national facility within Lawrence Berkeley National Laboratory that generates high intensity light for scientific and technological research. ALS currently has 32 operational beamlines [Advanced Light Source] allowing research projects in many different areas to be carried out at the same time. The beamline of interest in this research is the IR Beamline 1.4.3.

The IR Beamline is very sensitive to microscopic motion of the ALS beam. Despite extensive passive noise remediation efforts for the low frequency noise coming from vibrations of pumps and other sources on the ALS floor, the IR Beamline still had low frequency ($<500\text{ Hz}$) noise spikes. An optical feedback system was implemented to address the low frequency noise and reduce the beam motion [McKinney, 1999]. Figure 9 is a schematic of the active feedback system for the IR Beamline 1.4 complex.

The first tip/tilt mirror reflects the collimated IR beam from the ALS switchyard. The light then goes through the first beamsplitter, which reflects nearly 100% of the infrared light, but allows approximately 50% of the visible light to pass through to the PSD. The signal from the PSD is processed by a custom built analog circuit and provided as input to the first PZT tip/tilt stage. The

reflected light from the first beamsplitter goes to the second tip/tilt mirror where it is reflected through two more beamsplitters and onto the second PSD. The signal from this PSD is processed through another analog circuit and sent to the second PZT tip/tilt stage.

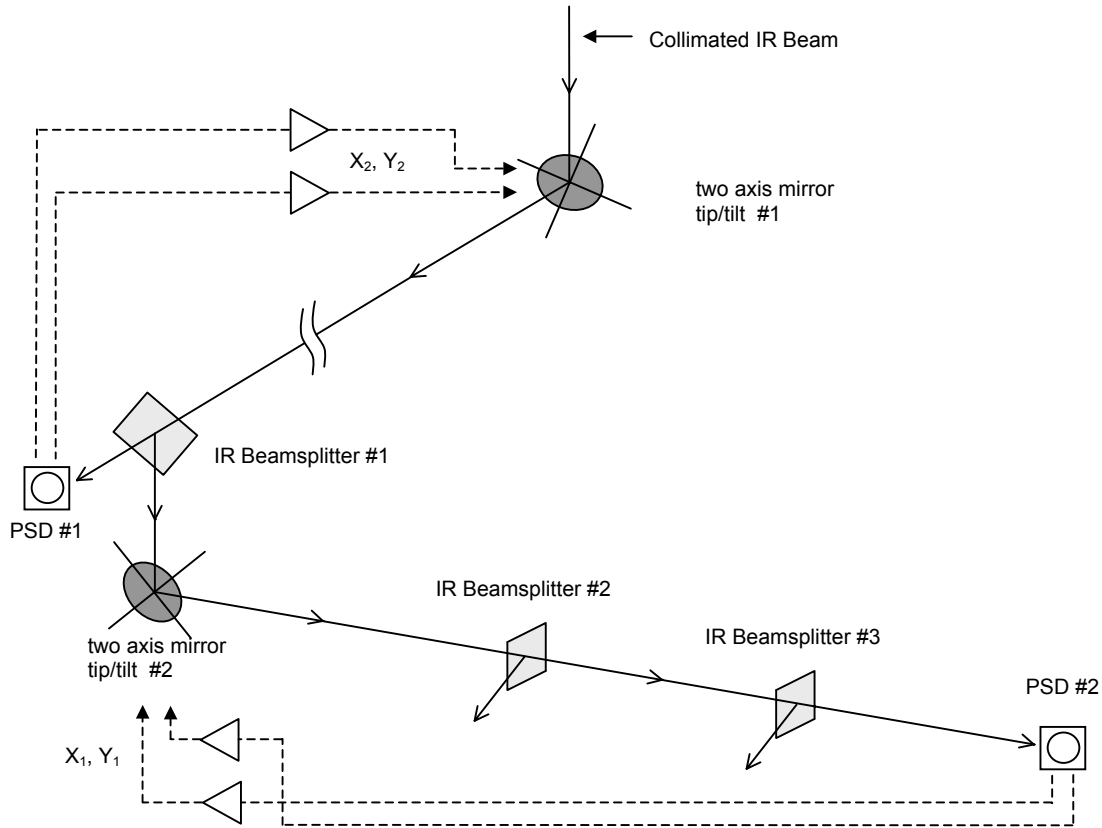


Figure 9. Active Mirror Feedback System for IR Beamlne 1.4 Complex.
From [McKinney, 1999]

The two stages allow the active feedback system to pin the beam at two positions to approximately $1 \mu\text{m}$, thus stabilizing the beam in both position and angle. Implementation of the 4-axis feedback system reduced the noise error signal from the primary vibrational resonance ($\sim 80\text{Hz}$) by approximately an order of magnitude and achieved a 5-fold decrease in the overall noise rms variation [McKinney, 2000].

D. KEK PARTICLE ACCELERATOR

In 1988, the High Energy Accelerator Research Organization (KEK) in Ibaraki, Japan, constructed a test facility to investigate alignment techniques for the Japan Linear Collider. The facility consisted of a stabilized laser system and a vibration control stage equipped with piezo transducers. The goal of the test facility was to develop a sub-micron alignment system for future positron-electron colliders to maintain a vertical beam size at the interaction point as small as 2 nm [Ishihara]. Ground motion measured at the KEK facility was on the order of 100 nm . The high frequency components were easily reduced by using conventional damping methods, however, an active alignment system was needed for frequencies below 10 Hz .

KEK began is fundamental study to understand the control system by building a one-dimensional alignment system using a laser interferometer and piezo transducers (Figure 10). The initial goal was to keep a stable distance, up to a maximum of 1 m , as accurately as 50 nm . For the laser interferometer system, they chose a separate-function laser system in which the interferometer is connected by fiber cables to a laser generator and to a fringe counter.

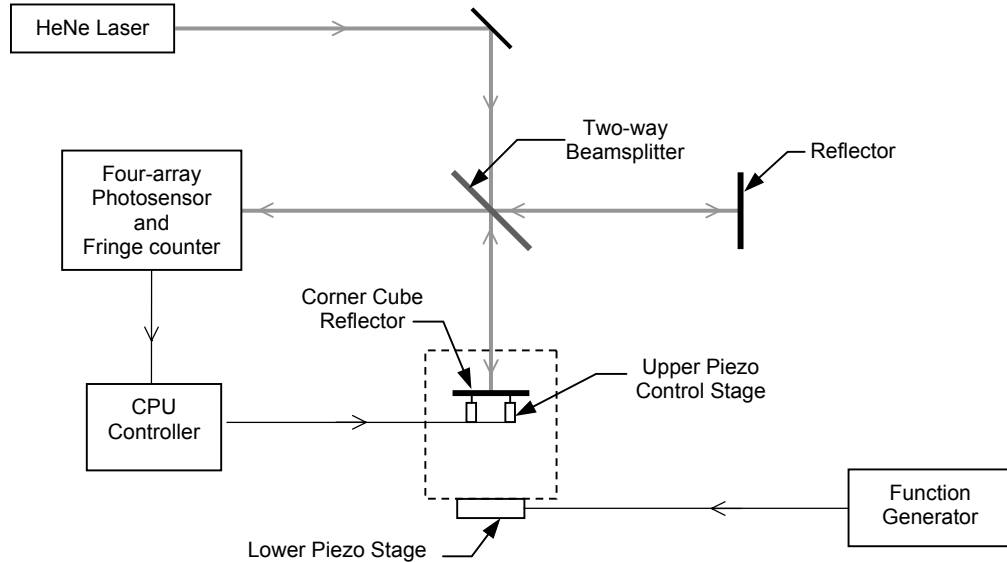


Figure 10. Block Diagram of the One-Dimensional Alignment System at KEK. Adapted from [Ishihara]

The laser system is based on the Michelson type interferometer. The laser beam goes through a two-way beamsplitter where one beam goes to a built-in reflector and the other to a corner cube mounted on the upper control stage. Beams coming from both reflectors make interference fringes on a four-array photosensor, measuring the distance from the interferometer head and the corner cube. The signal from the photosensor array is sent to a CPU controller that calculates the counteraction required to keep the corner cube stable, then drives the upper stage piezo transducers to achieve the desired counteraction. The test alignment system has two control stages, both controlled by Physik Instrumente piezo transducers model P-841.20. The upper stage controls the corner cube from which the distance is measured; the lower stage provides a disturbance to the upper stage with an arbitrary waveform.

The first test of the KEK's initial alignment system showed that the one-dimensional control system was able to keep a distance of 28 cm stable to better than 50 nm , up to a frequency of 20 Hz , against a sine wave disturbance with a 500 nm amplitude [Ishihara].

While this system is not an active mirror alignment system, it describes a possible method of maintaining active control of the FEL optical cavity length which must be kept stable to within $1\mu\text{m}$ [Colson, December 2002].

E. AIRBORNE LASER (ABL)

The U. S. Air Force is currently developing the Airborne Laser designed to destroy enemy missiles shortly after launch. The ABL employs both passive and active alignment systems for their optical equipment. CSA Engineering, Inc. is developing a vibration isolation system based on pneumatic vibration isolators. The isolator system suspends optical benches from the airframe to isolate them from structure borne vibrations.

The laser for this system is a mega watt-class chemical oxygen-iodine laser (COIL) currently being developed by TRW. Initial contact with TRW [Jackson, 2002] has indicated that the airborne laser will employ many active

optical alignment systems. As of this writing, I am still waiting for specifics on their optical cavity mirror alignment system.

F. BOEING VISIBLE FEL FACILITY

Towards the end of my research, I came across another FEL active mirror stabilization system employed by Boeing for use in their visible free electron laser experiments, and designed and implemented in cooperation with Spectral Technology, Inc. The stabilization system uses an electro-optic servo system with three main functional areas: a sensing system to detect the state of the system, an analog circuit to determine corrections to that state, and a device to provide the mechanical response of the system.

The angular position of the mirror is sensed through the use of a reference light source and a quadrant photodiode detector. The error signal from the detector is then processed by an analog circuit and amplified to drive the actuators on the mirror mounts. The mirror mount actuators are small voice coil type devices. For a more detailed description of the stabilization system, see Shemwell, "Optical Cavities for Visible Free Electron Laser Experiments" [Shemwell].

V. CONTROL THEORY

In this chapter, we consider the feedback control theory of the motion of a laser mirror due to random vibrations. For laboratory as well as shipboard environment applications, the frequency of the vibrations will be low, by which we mean that the mirror itself can be considered as a rigid body. Hence, we do not consider adaptive optics techniques. For simplicity, we assume only one translational degree of freedom. Extension to orthogonal uncoupled degrees of freedom is immediate. The model system is discussed in Section A, stability in Section B, control of steady state vibrations in Section C, and control of transient vibrations (shocks) in Section D.

There are many books that include control theory (refer to the bibliography). A variety of sophisticated techniques have been developed. However, we will show that the solution to the problem of the control of single-degree-of-freedom vibrations is particularly straightforward, and is best handled simply by use of the basic properties of a damped driven harmonic oscillator. It is surprising that we did not find this solution in any of the books dealing with control theory.

A. MODEL SYSTEM

We make the plausible assumption that the combination of the mirror, mirror mount, and controlling actuator that is attached to the mirror acts as driven damped mass on a spring (Figure 11). Other mechanical resonances may be present in an actual system, but it may be possible to identify these and add stiffness such that their resonance frequencies are pushed to sufficiently large values that the response is negligible. In Figure 11, it should be noted that the actuator represents an ideal element that exerts an instantaneous force proportional to the instantaneous input voltage. The actual inertia, stiffness, and damping are considered to be lumped into the mass m , spring constant k , and

damping coefficient c_d , respectively. We develop the theory for longitudinal motion, but it immediately applies to rotational motion.

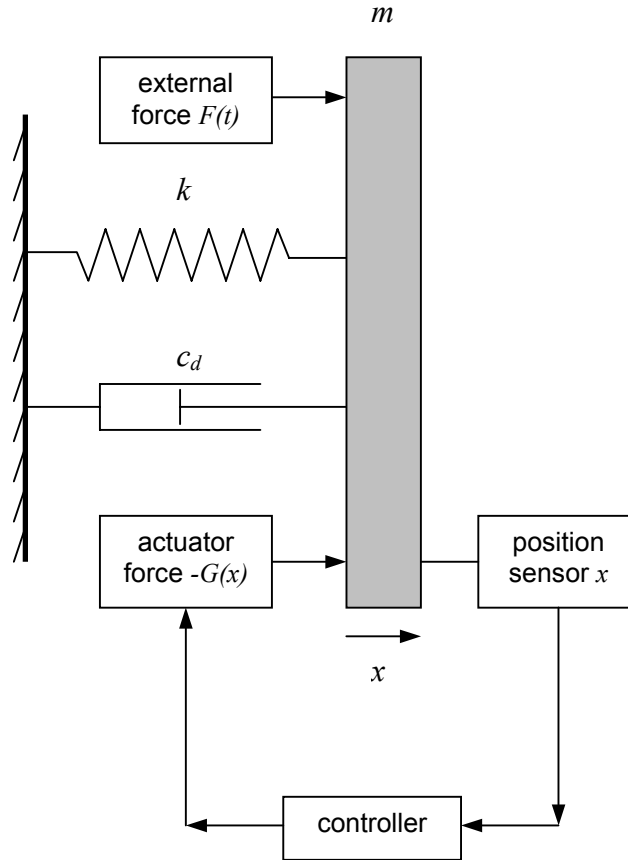


Figure 11. Model System with a Single Degree of Freedom. The objective is to determine the force $G(x)$ such that the vibrations of m due to the force $F(t)$ are minimized.

The equation of motion for the displacement $x(t)$ of the mass m from equilibrium is

$$m\ddot{x} = -kx - c_d\dot{x} + F(t) - G(x) ,$$

where $F(t)$ is the external force and $G(x)$ is the force due to the actuator. The equation of motion in standard form is then

$$\ddot{x} + 2\gamma\dot{x} + \omega_o^2 x = \frac{1}{m}F(t) - \frac{1}{m}G(x) , \quad (28)$$

where the damping parameter is $\gamma = 2/c_d m$ and the natural angular frequency is $\omega_o = (k/m)^{1/2}$.

We show in Sections C and D that an appropriate form of actuator force in our case is

$$G(x) = \alpha x + 2\beta\dot{x} . \quad (29)$$

This amounts to a gain of α applied to the displacement and a gain of β applied to the velocity, where α has dimensions of force/displacement and β force/velocity.

The most common controller is by far the PID type, where “P” stands for proportional, “I” for integral, and “D” for derivative. In this terminology, P refers to a term proportional to the signal, I refers to a term proportional to the integral of the signal, and D refers to a term proportional to the derivative of the signal. The case in Eq. (29) thus corresponds to a PD controller.

Substituting Eq. (29) into Eq. (28), and combining the displacement and velocity terms, yields

$$\ddot{x} + 2\Gamma\dot{x} + \Omega^2 x = \frac{1}{m}F(t) , \quad (30)$$

where the square of the effective natural angular frequency is

$$\Omega^2 = \omega_o^2 + \frac{\alpha}{m} = \frac{k + \alpha}{m} , \quad (31)$$

and the effective damping parameter is

$$\Gamma = \gamma + \frac{\beta}{m} . \quad (32)$$

From Eq. (31), the effective stiffness is

$$K_E = k + \alpha . \quad (33)$$

An important aspect of the actual system is that direct experimental analysis can confirm the model in Figure 11 (or perhaps allow it to be enforced by appropriate alteration of the system), and the parameters quantified. This can be accomplished by removing the external force, disconnecting the displacement sensor from the controller, and driving the controller with source of a dynamic signal analyzer that is also connected to the sensor. If the external force cannot be removed, then the source of the analyzer may be increased such that it dominates the external force. The analyzer is made to slowly sweep through frequencies of interest. This “swept sine” analysis yields frequency response curves, from which all necessary data can be determined.

B. STABILITY

Positive feedback typically leads to unstable growth in controlled systems. Any phase lag from the sensor to the actuator in Figure 11, must therefore be carefully considered. Experimental tests (Chapter. VI) show that there is no phase lag due to the controller even to frequencies of many kilohertz. Because it is optical, the sensor is expected to have the same property. Recall that the actuator in Figure 11 is ideal; any inertia, stiffness, or damping is incorporated into the parameters m , k , and c_d . Hence, there is no phase lag associated with the actuator in Figure 11.

Initially, we naively thought that the fact that the phase lag of x relative to F is less than 180° (Section C) was fortuitous in that positive feedback would be avoided. However, the phase shift between x and F is irrelevant in our system,

because the control acts on the stiffness and damping, as shown in the equation of motion (Eq. 30).

Positive feedback in our system corresponds to negative values of the gains α and β in the actuator force (Eq. 29). This serves to lower the stiffness and damping, respectively, as shown in the equation of motion (Eq. 30) together with the effective stiffness (Eq. 33) and effective damping parameter (Eq. 32). The stability criteria for our system is that the effective stiffness $k + \alpha$ and effective damping parameter $g + \beta/m$ are positive, or

$$\alpha > -k \quad \text{and} \quad \beta > -\gamma m \quad (34)$$

Positive velocity feedback (negative β) for our system might conceivably be required (Section D), which is allowed as long as the gain conforms to the stability requirement (Eq. 34).

C. CONTROL OF STEADY-STATE VIBRATIONS

For a monofrequency driving force $F = F_o \cos(\omega t)$, the steady-state solution of the equation of motion (Eq. 30) is well-known [Fowles]. The displacement is $x(t) = A \cos(\omega t - \varphi)$ where the amplitude A and phase lag φ are

$$A = \frac{F_o/m}{\sqrt{(\Omega^2 - \omega^2)^2 + 4\Gamma^2\omega^2}}, \quad (35)$$

$$\varphi = \tan^{-1} \left(\frac{2\Gamma\omega}{\Omega^2 - \omega^2} \right). \quad (36)$$

Figure 12 shows graphs of the steady-state amplitude and phase as functions of the drive frequency ω for constant force amplitude F_o and for different values of the damping parameter Γ .

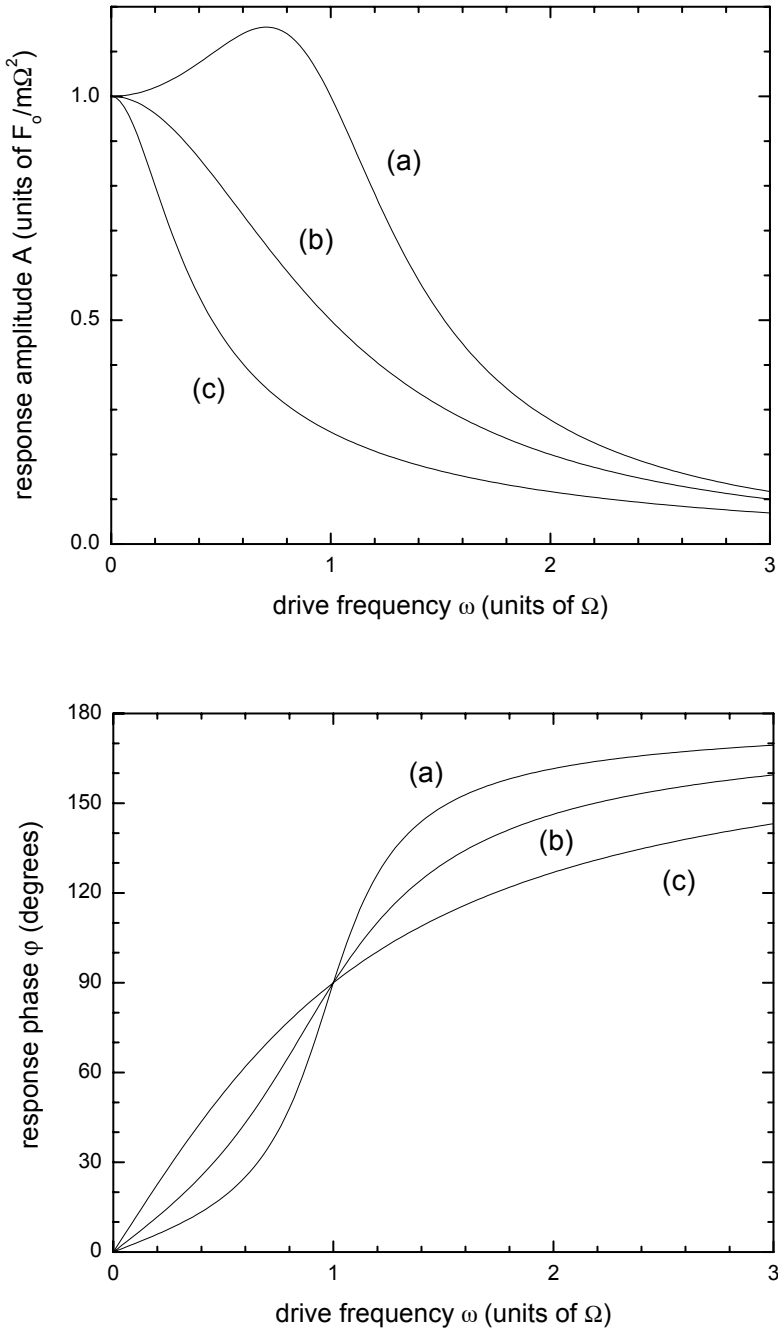


Figure 12. Model System Steady-State Response. The graphs show steady state response amplitudes and phases of a driven damped oscillator as a function of the drive frequency for the cases of (a) underdamping, $\Gamma < \Omega$; (b) critical damping, $\Gamma = \Omega$; and (c) overdamping, $\Gamma > \Omega$. The underdamped case is $\Gamma = \Omega/2$, and the overdamped case is $\Gamma = 2\Omega$.

In Section D, we show that the control of abrupt (transient) vibrations is best handled by adjusting the velocity feedback gain β in Eq. (29) so that the effective damping parameter Γ in Eq. (32) is the critical value $\Gamma = \Omega$. This corresponds to the intermediate [i.e., (b)] curves in Figure 12. The maximum displacement occurs in the limit of zero frequency (*stiffness-controlled regime*), and is given by $F_o/m\Omega^2 = F_o/K_E$, where K_E is the effective stiffness (Eq. 33). The displacement is minimized by choosing the largest possible value of K_E , which occurs for the largest possible value of the displacement gain α in Eq. (29). The maximum displacement, which corresponds to the displacement at zero frequency, is

$$x_{\max} = \frac{F_o}{k + \alpha} . \quad (37)$$

The maximum displacement can be made as small as desired by choosing the displacement gain α to be sufficiently large according to Eq. (37). It should be noted that, even if there was underdamping rather than critical damping, one would still choose the largest possible value of α in our case, in order to push the resonance to higher frequencies such that the amplitude of external vibrations is negligible.

D. CONTROL OF TRANSIENT VIBRATIONS

To consider the effect of transient vibrations (shocks), we investigate the equation of motion (Eq. 30) for an abruptly applied force:

$$F(t) = \begin{cases} 0, & t < 0 \\ F_o, & t > 0 \end{cases} ,$$

where F_o is a constant, and where the mass is initially at rest in equilibrium. The solution $x(t)$ to Eq. (30) can be readily obtained. By Hooke's law, the particular solution is just the infinite time equilibrium value, which is the force divided by the effective stiffness (Eq. 33), or $x(\infty) = F_o/m\Omega^2$ by Eq. (31).

In the case of underdamping ($\Gamma < \Omega$), the homogeneous solution [Fowles] has terms proportional to $e^{-\Gamma t} \cos(\Omega_d t)$ and $e^{-\Gamma t} \sin(\Omega_d t)$, where the damped angular frequency is

$$\Omega_d = \sqrt{\Omega^2 - \Gamma^2} .$$

Implementing the initial conditions of zero displacement and zero velocity in the general solution yields

$$x(t) = \frac{F_o}{m\Omega^2} \left\{ 1 - e^{-\Gamma t} \left[\cos(\Omega_d t) + \frac{\Gamma}{\Omega_d} \sin(\Omega_d t) \right] \right\} . \quad (38)$$

Critical damping has $\Gamma = \Omega$ or $q = 0$. In this case, the homogeneous solution [Fowles] has terms proportional to $e^{-\Omega t}$ and $te^{-\Omega t}$. Implementing the initial conditions in the general solution yields

$$x(t) = \frac{F_o}{m\Omega^2} \left(1 - e^{-\Omega t} - \Omega t e^{-\Omega t} \right) . \quad (39)$$

In the case of overdamping ($\Gamma > \Omega$), the homogeneous solution [Fowles] has terms with exponential decay constants given by $\Gamma \pm q$, where

$$q = \sqrt{\Gamma^2 - \Omega^2} .$$

Implementing the initial conditions yields

$$x(t) = \frac{F_o}{m\Omega^2} \left[1 - \frac{\Gamma+q}{2q} e^{-(\Gamma-q)t} + \frac{\Gamma-q}{2q} e^{-(\Gamma+q)t} \right]. \quad (40)$$

Figure 13 shows graphs of $x(t)$ for the three different cases Eqs. (38), (39), and (40). We confirm what is often claimed without proof in mechanics textbooks: Critical damping leads to the quickest approach to equilibrium. We thus adjust β in Eq. (29) such that the total damping parameter Γ in Eq. (32) has the critical value $\Gamma = \Omega$. It is conceivable that β may be negative, which would occur when γ is greater than the critical value. This does not cause a problem even though the feedback is positive rather than negative in this case (Section B). The motion will be stable as long as the effective damping parameter Γ is positive [refer to the stability requirement (Eq. 34)]. It should be noted that, because Γ will be adjusted to be large (Section C), it is unlikely that β will be negative.

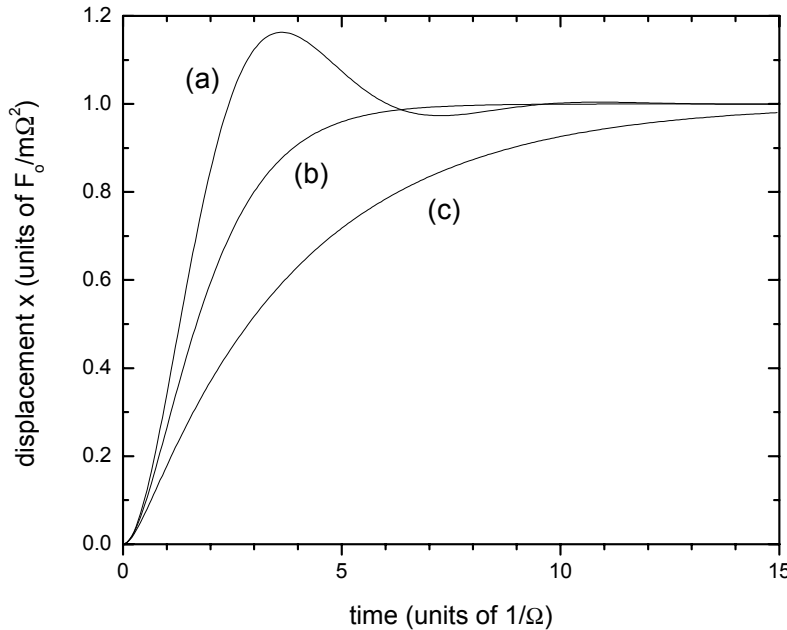


Figure 13. Response Curves of a Damped Driven Oscillator. Responses of a damped oscillator subject to a step function drive $F(t < 0) = 0$ and $F(t > 0) = F_o$. The oscillator is initially at rest in equilibrium. The cases are: (a) underdamping, $\Gamma = \Omega/2$; (b) critical damping, $\Gamma = \Omega$; and (c) overdamping, $\Gamma = 2\Omega$.

THIS PAGE INTENTIONALLY LEFT BLANK

VI. ACTIVE MIRROR ALIGNMENT EXPERIMENT

The purpose of the experimental alignment system is to understand the underlying physics of active feedback control theory. The knowledge gained from the study of this initial system will be used as a basis for follow-on research leading towards the development of a prototype active mirror alignment system for shipboard free electron lasers.

A. BASIC DESIGN AND COMPONENTS

In general, in a feedback system a specific physical quantity is being controlled. The control is achieved by making a comparison of this quantity with its desired value and using the difference to reduce the error. In our system, a laser is reflected from a piezo-electrically controlled mirror (PZT) to a position sensing detector. The desired position of the beam spot is in the center of the detector (reference value 0V). The actual position of the beam (detector output signal) is sent to a control circuit which conditions the signal and then sends it to the piezo actuators that move the mirror such to reduce the error. A block diagram of the system is shown in Figure 14. The three main components (detector, mirror mount and reference laser) are mounted on a floated optical bench.

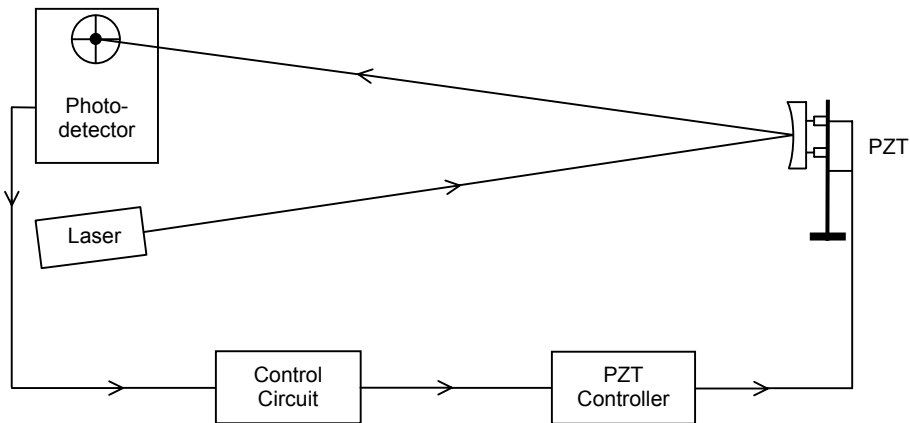


Figure 14. Block Diagram of the Experimental Alignment System.

Table 1 is a list of main components used in the experimental mirror alignment system.

COMPONENT	MANUFACTURER	PART NUMBER
Laser Diode Kit	Thorlabs, Inc.	S2001
Piezo-electric Kinematic Mount and Driver	Thorlabs, Inc.	PZ630
1" Metal Mirror Protective Aluminum Coating	Thorlabs, Inc.	PF10-03-G01
Quad Photodiode	Pacific Silicon Sensor, Inc.	PSS-QP50-6SD

Table 1. Experimental Alignment System Components.

1. Position Sensing Detector

The input signal of our system is provided by a position sensing detector, which we chose to be a four-element quadrant detector (quad photodiode). The advantage of using a quad photodiode is that it provides a null signal (0V) at the center of the detector. The null signal is used as the reference value in the feedback control loop. The detector used is the QP50-6SD manufactured by Pacific Silicon Sensor, Inc. The QP50-6SD is composed of a quad photodiode array and associated circuitry with current-to-voltage sum and difference amplifiers. A block diagram is shown in Figure 15. The output voltages are obtained by sending the diode element currents into current-to-voltage amplifiers with a gain of 10^4 .

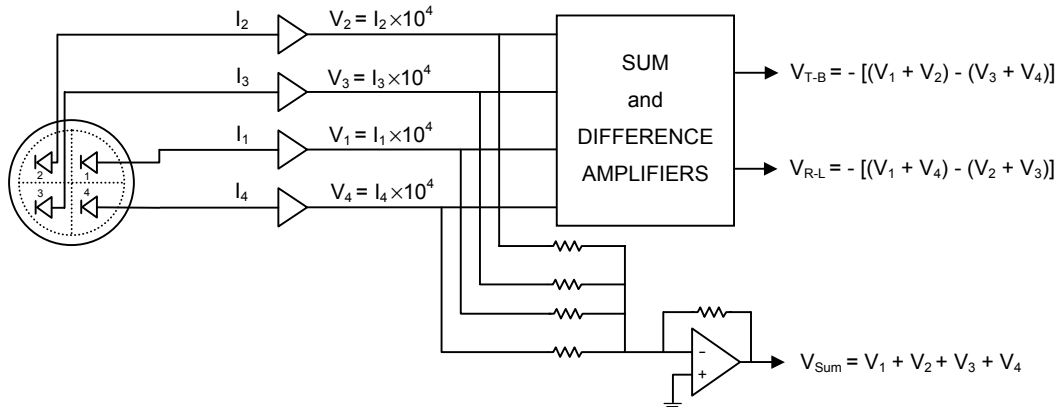


Figure 15. Quad Photodiode Block Diagram. From [Pacific Silicon]

In a quad photodiode, the position of the centroid of light is determined by comparison of the signals from the four quadrants. The vertical displacement is given by the top minus bottom difference signal (V_{T-B}) and the horizontal displacement from the right minus left difference signal (V_{R-L}). Additionally, the QP50-6SD provides a signal that is the sum of all four quadrant diode signals. This was not used in the experiment. The difference signals are voltage analogs of the light intensity difference sensed by the pairs of photodiode elements in the array.

2. Actuator System

Since the actuator system acting upon the mirror must have extremely fine resolution to counteract the vibrations, piezoelectric actuators were chosen. The actuator system used is a Piezoelectric Kinematic Mount made by Thorlabs, Inc. The Piezoelectric Kinematic Mount combines the mechanical features of a kinematic mirror mount (3 independent coarse manual adjuster screws) and the electro-mechanical features of a piezoelectric stack. The piezoelectric stacks are mounted in the front plate directly under the tips of three mirror adjuster screws. This allows for a coarse and fine control of both the translation and the angle of the mirror. The piezoelectric actuators have a 30 arc sec angular range and an $8 \mu\text{m}$ translational range, with an angular resolution of 0.06 arc sec , giving the

actuators $150 \mu\text{rad}$ control over angular range and an angular resolution on the order of $0.3 \mu\text{rad}$.

The actuators are controlled by a precision 3-channel piezo controller (Thorlabs MDT630). The controller allows each of the three piezo actuators to be controlled independently. The external drive voltages can be supplied by any stable voltage source (from 0 to 10V). In our system, the drive voltage signal comes from the position sensing detector. The piezo drive controller also allows for precise manual settings of the output by use of a precision 10-turn potentiometer. Since both the manual control and the external input voltages are summed, the manual control can be used for offset adjustments without having to readjust the external voltage source.

3. Reference Laser

The reference laser (Thorlabs S2011) is a class IIIb 4.5mW adjustable focus diode laser. The S2011 laser kit includes the laser module, DC power supply and mounting hardware. The laser module has an internal constant-power driven circuit to regulate the output power to better than 99.5%. The laser is mounted on a kinematic mount which provides stable pointing alignment of the laser.

4. Control Circuit

The control circuit conditions the signal before input to the piezo actuators. For the initial phase of the experiment we started with a basic proportional control circuit. We later added a derivative control to the circuit. The output from the quad photodiode is first filtered and then a gain is applied to the signal which is fed to the piezo driver to control the piezo actuators. Since the quad photodiode did not come with a power supply or output connectors, we designed a control box to provide required power and added a 7-pin quick disconnect and bnc output connectors to simplify its use. The control box also has internal circuitry to bring the quad output voltages ($\pm 12\text{V}$) to the required input range of the piezo

driver (0 to 10V). However, the internal circuitry was not used for the initial tests. We chose instead to use the voltage off-set feature of the piezo driver. Figure 16 is the control box schematic.

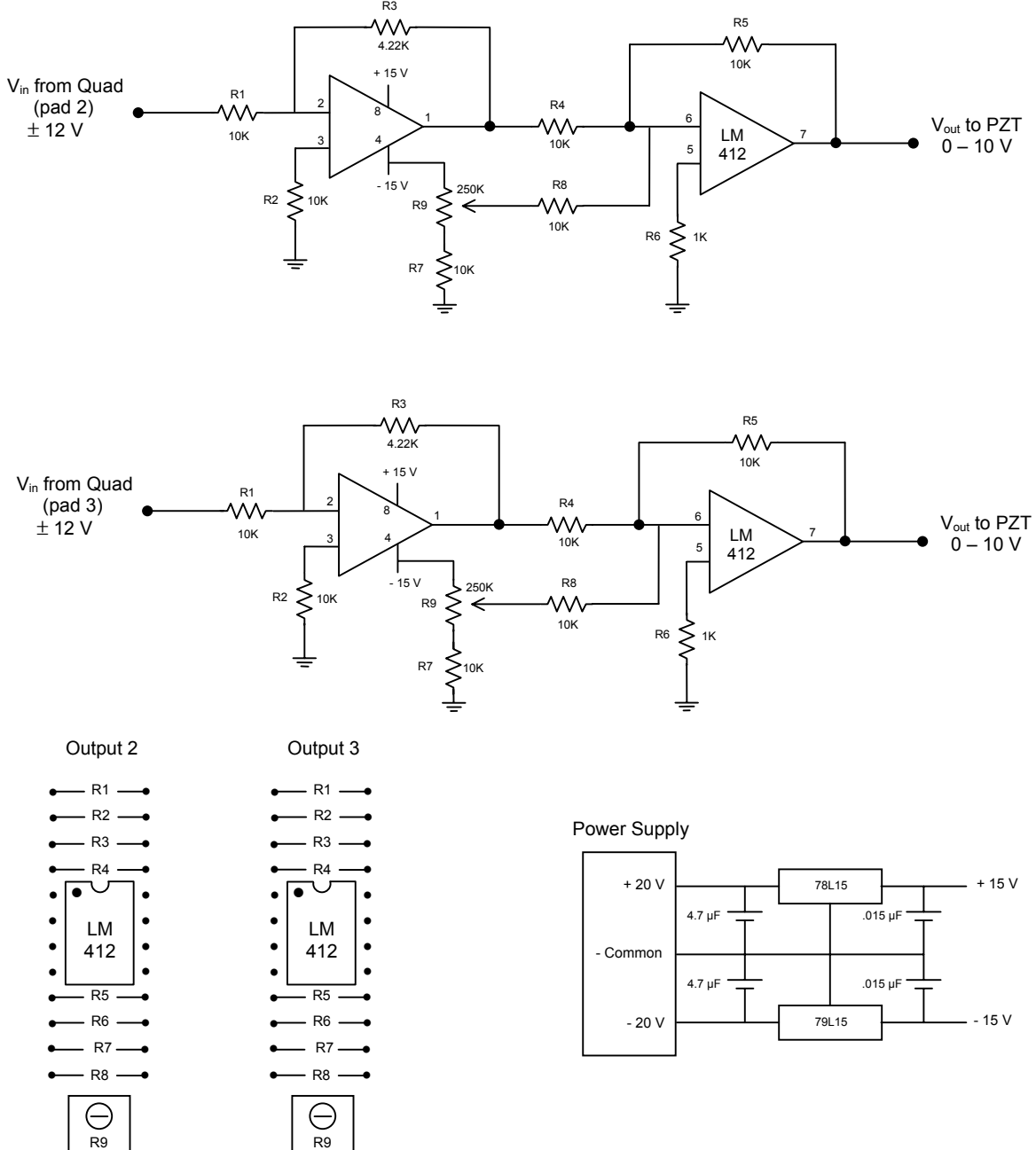


Figure 16. Schematic of Quad Photodiode Control Box. The control box includes two voltage offset circuits, one for each summing/difference output of the quad, and a power supply offset ($\pm 20V \rightarrow \pm 15V$).

A diagram of the final control circuit is shown in Figure 17. (For more information on intermediate tests of the control circuit, see RESULTS.)

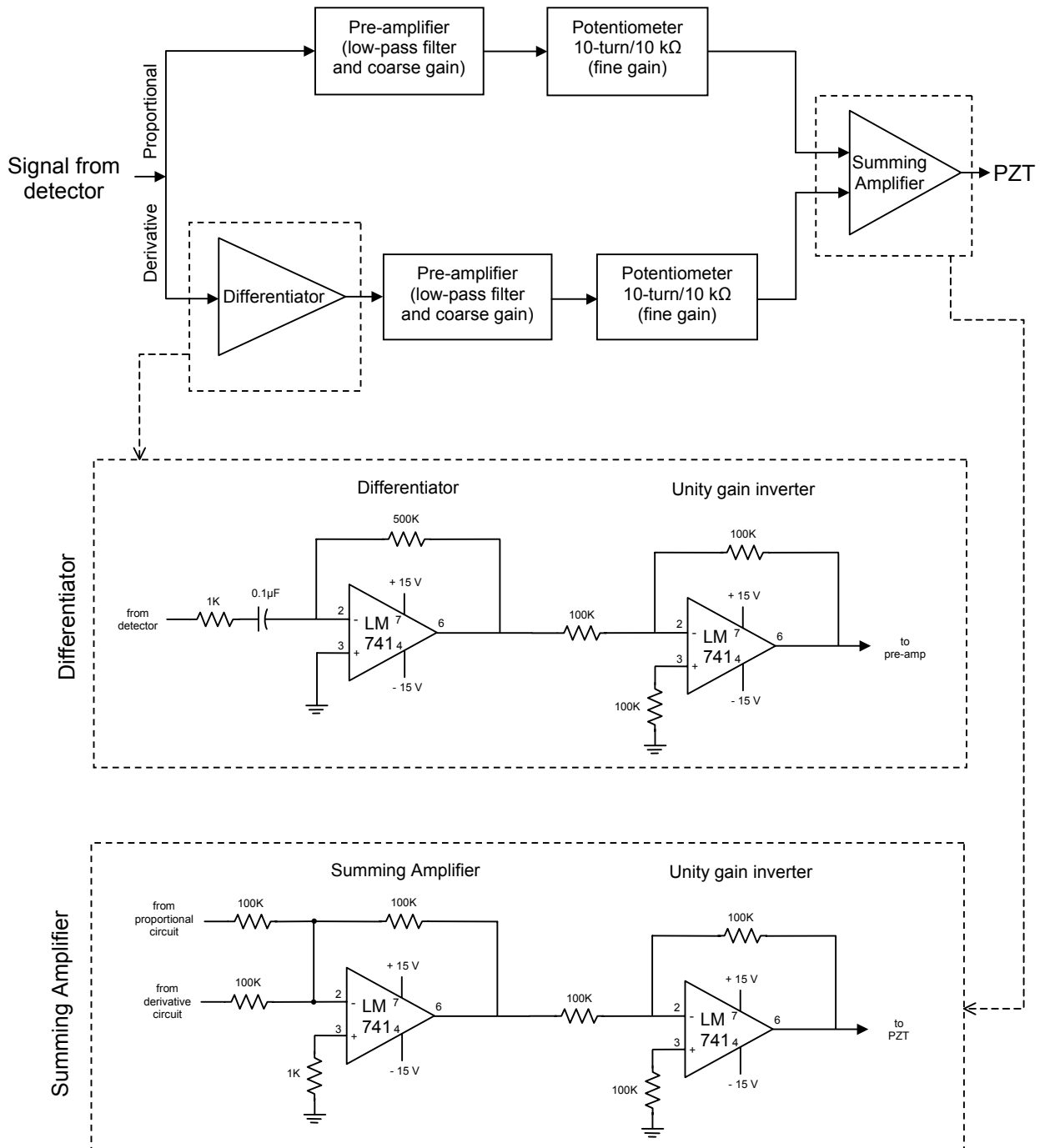


Figure 17. Proportional - Derivative Control Circuit Diagram

B. RESULTS

The first experiment we did was to test the piezo controller. We provided an external signal with a function generator and monitored both input and output on an oscilloscope. Our input was a 0.2V peak-to-peak (p-p) sine wave and the observed output was a 3V p-p sine wave. This observation confirmed the manufacturer's specification of an output gain of 15. We also characterized the controller as a function of frequency. We observed no detectable phase shift for a frequency sweep from 10 Hz to 10 kHz.

Next we tested the kinematic mirror mount. Each piezo was connected to the piezo controller and the driving voltages were provided manually using the precision 10-turn potentiometers. We observed the mirror displacement by reflecting the laser from the mirror to a wall. The laser spot was observed to move as indicated by the manufacturer as we manually drove each piezo.

Next we performed a preliminary characterization of the piezo-electric kinematic mount by reflecting the laser from the mirror to the detector and analyzing the signal from the photodiode with a signal analyzer. First we set a 75V output manual off-set on the piezo driver (middle of piezo operation range) and manually centered the beam on the detector using the adjuster screws on both the laser mount and the kinematic mount. The output from the detector was observed on a signal analyzer. The first resonance of significance was at 120 Hz, then a very strong resonance around 330 Hz and another one around 970 Hz. The first was due to vibrations of machinery in the building. The second two were evidently modes of the mirror mount.

1. Proportional Control

For the initial test of the feedback loop, we simply fed the output from the detector directly to the piezo controller. The output from the detector was monitored on both an oscilloscope and a signal analyzer. Before feeding the signal we verified that if the mirror were to tilt forward, the beam would move slightly below the center of the detector and give a negative voltage to the piezo

driver thus causing the actuators to tilt the mirror back. After completing the feedback loop, we were unable to detect any notable difference in the signal. We then decided to drive one of the piezos with a definite frequency and control the system by directly feeding the output signal to one of the other piezos (the third piezo was held fixed). We drove the piezo with a 20 Hz, 500 mV p-p sine wave. Before completing the feedback loop, we first checked the system response against the drive input. The response matched the drive with no significant phase shift from 20 to 200 Hz, slight phase shifts at 240 and 330 Hz, and approximately 90° phase shifts at 430 and 760 Hz. We then fed the detector output to the piezo driver. As soon as we fed the signal to the piezo driver, the system responded with immediate positive feedback and went into self-oscillation.

Our first attempt to eliminate the positive feedback was to filter out frequencies above 200 Hz with a Bessel filter. After installing the filter, we were able to maintain negative feedback and stabilize the system. With this configuration we achieved a system response reduction by a factor of approximately 1.5.

From our model system (Chapter V), we showed that applying a gain to the output signal would reduce the system response. Therefore, in our next test of the system we added a gain to the output signal. The gain was provided with a power amplifier using a manual potentiometer. The gain stage was applied to the signal after the filter and before the input to the piezo controllers. With this system configuration we were able to further reduce our response to slightly better than a factor of 2. In summary, the system response to the 500 mV disturbance was a 245 mV p-p sine wave with no feedback, and was reduced to 115 mV p-p with the feedback on (filter and gain). Although we were able to achieve a factor of 2 reduction in system response by installing a filter and applying a gain to the signal, as we continued to increase the gain beyond that result, the system went into positive feedback and self-oscillation. There is thus a 180° (or at least a sufficiently large) phase shift in the control circuit. This result

goes against the theory in our model system. According to our model, the response should continue to decrease as the gain is increased. The model system may thus need to be modified. Figure 18 shows the response of the system, first with feedback off (0mV) and with feedback on (300 mV).

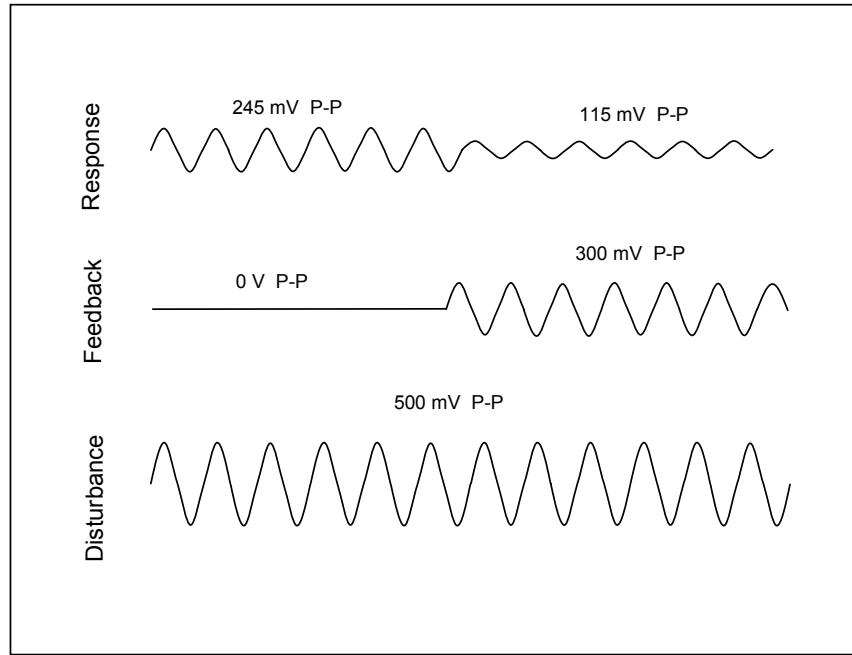


Figure 18. Schematic of System Response with Initial Control Circuit.

Disturbance provided by a 20 Hz, 500 mV p-p sine wave. With feedback off (0V) the response is 240 mV p-p. With feedback on (300 mV) the response decreases to 115 mV p-p.

The first step in understanding this behavior was to try to identify the cause of the phase shift and thus determine the source of the instability. Because filters introduce phase shifts, our first decision was to replace the 8-pole Bessel filter with a 6-dB low-pass filter using the single-pole filter of a low-noise preamplifier. We also replaced the gain stage power amplifier with a 10-turn potentiometer. After making the changes we were able to improve our previous results and achieve a factor of 3.5 reduction in system response. Figure 19 shows the system response with the second control circuit.

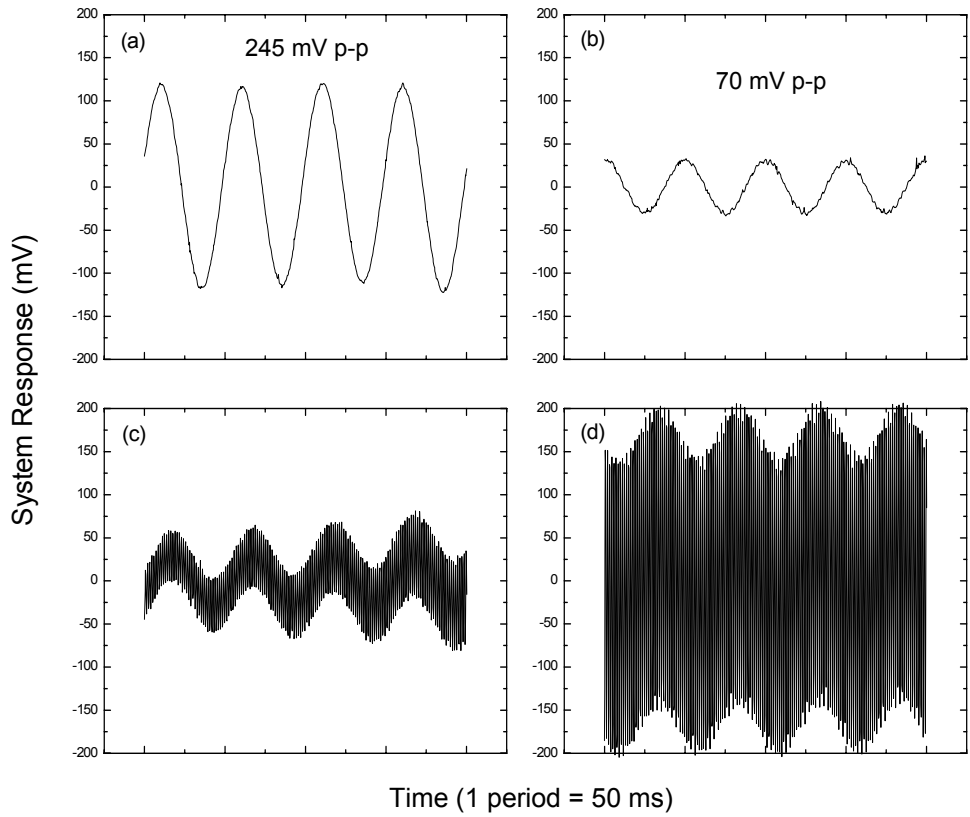


Figure 19. System Response with Second Control Circuit. System response to a 20 Hz, 500 mV p-p sine wave disturbance with (a) feedback off; (b) feedback on; (c) and (d) as system goes into positive feedback and self-oscillation.

However, as can be seen in Figure 19, the system is still unstable and goes into positive feedback and self-oscillation as the gain is increased. Our next step in trying to identify the phase shift was to determine at which frequencies the instability occurred. To measure the frequency as the system went into self-oscillation, we monitored the output signal with a signal analyzer while slowly increasing the gain. Results are shown in Table 2. The control circuit configuration indicates the type of filter and gain. It is interesting to note that without the Bessel filter, the system goes unstable at the same frequency (760 Hz) regardless of control circuit configuration. This frequency corresponds to a system resonance frequency.

Control Circuit Configuration	Instability Occurrence
Bessel Filter/ Power amplifier	98 Hz
No Filter/ Power amplifier	760 Hz
Low-pass Filter/ Preamp/potentiometer	760 Hz

Table 2. System Instability as a Function of Frequency.

2. Mirror Mount Characterization.

Our next step in identifying the cause of the phase shift was to characterize the actuator-detector system in terms of amplitude and phase as a function of frequency. The characterization was done in an open loop configuration using a swept sine mode on a signal analyzer (HP 35665A) for a frequency sweep from 1 Hz to 1kHz. Two separate sweeps were conducted, one to characterize the driven piezo, and the other for the controlled piezo. Results of the swept sine characterization are shown in Figures 20 and 21 for the previously driven and previously controlled piezo, respectively.

The results from the swept sine mode characterization of the piezo-electrically controlled mirror mount suggest that the instability and on-set of positive feedback may be caused by a coupling of the phase responses of the driven and controlled piezos. From Figures 20 (b) and 21 (b), we see that at around 760 Hz (frequency at which the system goes unstable), the phase shifts of the two piezos add to greater than 180°. The total phase shift could lead to the positive feedback and self-oscillation we observed during the initial tests of the experimental alignment system. Further analysis and interpretation of the data needs to be conducted to confirm this preliminary conclusion.

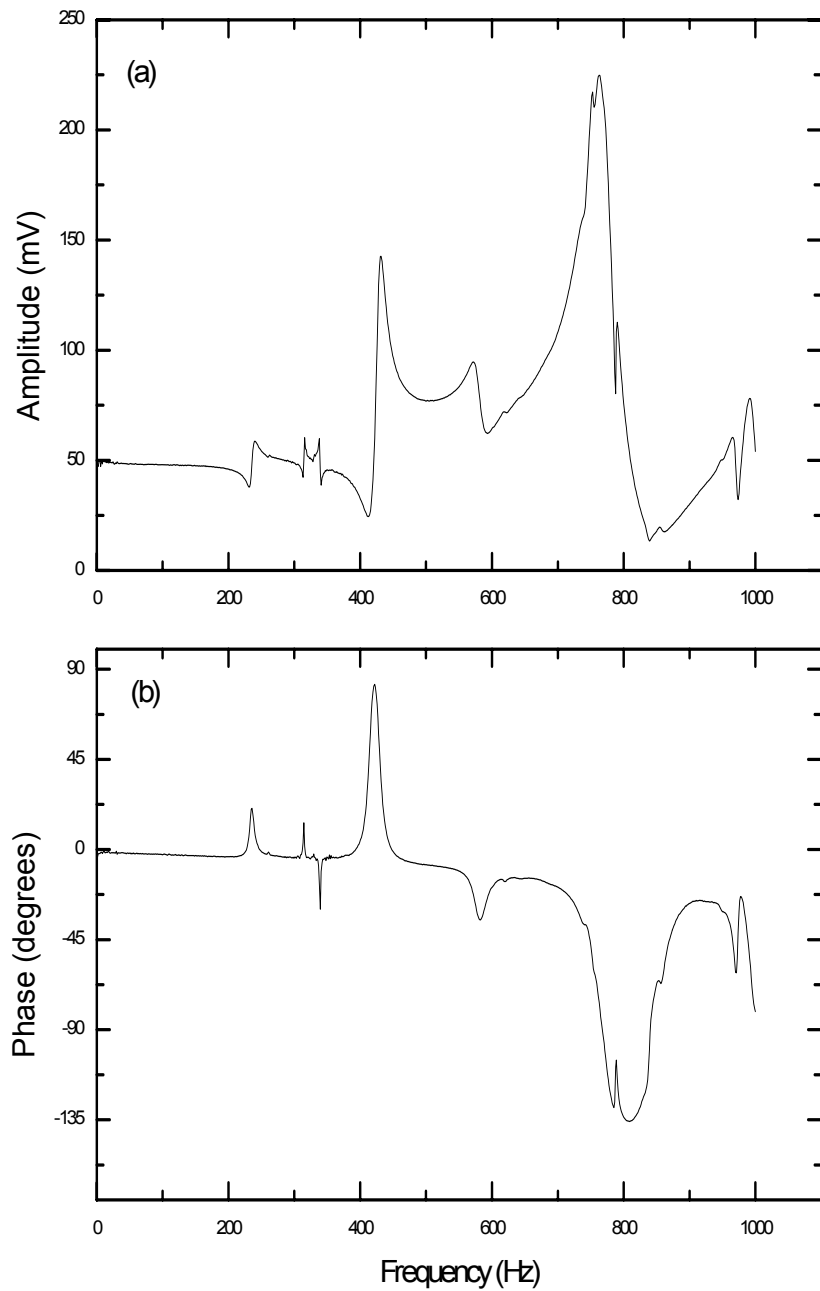


Figure 20. Mirror Mount (driven piezo) Characterization. Results of swept sine characterization in terms of amplitude and phase for a frequency sweep from 1 Hz to 1 kHz and a source level of 100 mV. Amplitude response is shown in (a) with a maximum peak amplitude of approximately 225 mV at around 760 Hz. Phase response is shown in (b) with a maximum phase shift of about 130° at approximately 800 Hz.

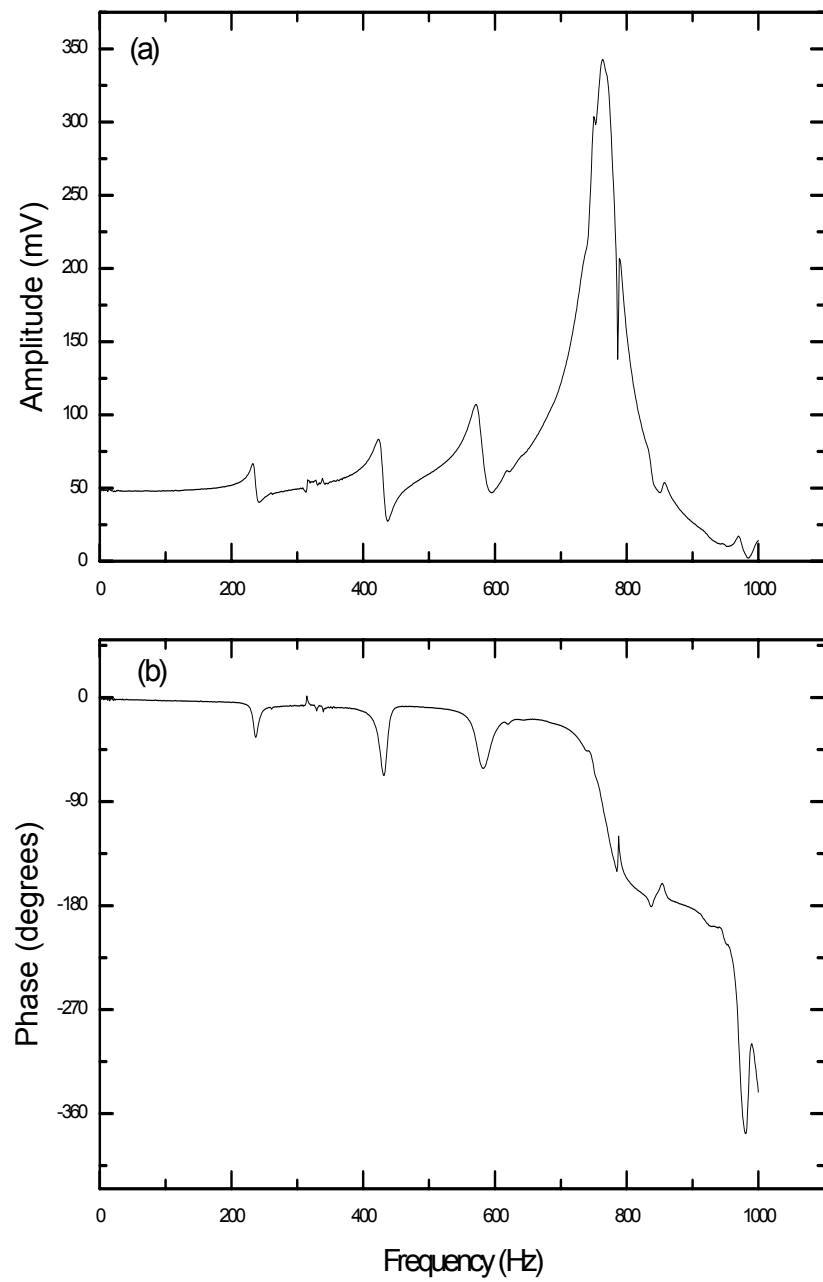


Figure 21. Mirror Mount (controlled piezo) Characterization.

Results of swept sine characterization in terms of amplitude and phase for a frequency sweep from 1 Hz to 1 kHz and a source level of 100 mV. Amplitude response is shown in (a) with a maximum peak amplitude of approximately 330 mV at around 760 Hz. Phase response is shown in (b) with a maximum phase shift of about 375° at approximately 960 Hz.

3. Proportional-Derivative Control

Our final test of the alignment system was to explore the effects of velocity feedback control by taking the derivative and applying a gain to the output of the detector to increase the damping in the system and therefore reduce the response (see Chapter V - Control Theory). We modified our control circuit to include a differentiator and summing amplifier to test the combination of the proportional and derivative feedback control on the alignment system.

We first tested the effect of applying a gain to the derivative of the signal without the proportional gain by zeroing out both potentiometers then slowly increasing the gain by turning only the potentiometer associated with the derivative. We observed a slight reduction in system response by a factor of approximately 1.3 before the system went unstable.

Next, we tested the entire proportional-derivative (PD) control circuit. As before, we started by zeroing out both potentiometers, then we increased the gain of the derivative until we reached the instability, then we backed-off until the system was stable. With the set derivative gain, we then increased the gain of the proportional signal. A slight gain in the proportional signal quickly produced an instability in the system response.

Our final step was to once again, zero out both potentiometers then increase the gain of the proportional signal until close to instability, but well within its stability range. We then slowly increased the gain of the derivative, but noticed no further reduction in system response.

Although we implemented the entire PD circuit, we achieved the maximum system reduction by zeroing out the derivative potentiometer and increasing the gain on the proportional signal. Our final result yielded a reduction by a factor of 5 in system response. Figure 22 shows our final result and maximum system response reduction.

Just before this thesis was submitted, we became aware that the above methodology for implementing a PD system is not complete. After setting P to an

intermediate value and increasing D, we should have been able to increase P again and improve the stability margin.

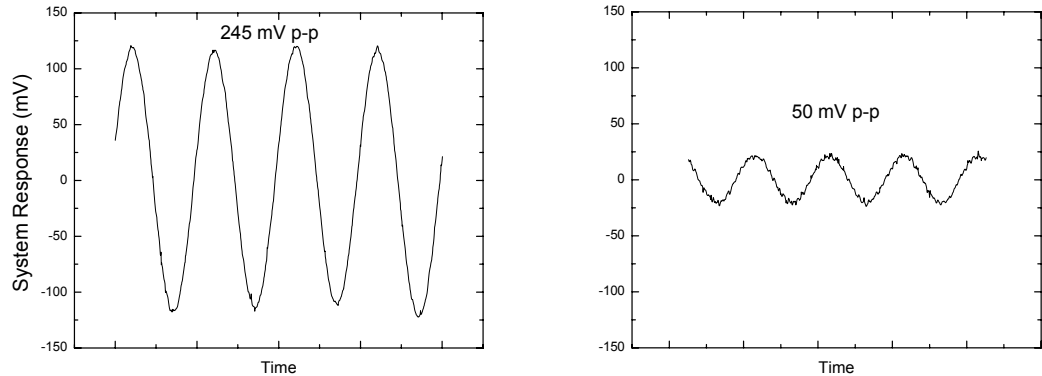


Figure 22. System Response with Proportional-Derivative Control.
These results show the system response without feedback control (a), and with implementation of the proportional-derivative feedback control circuit (b).

THIS PAGE INTENTIONALLY LEFT BLANK

VII. CONCLUSIONS AND FUTURE WORK

A. CONCLUSIONS

Investigation of laboratory FEL facilities, along with other high energy facilities, has shown that in the laboratory environment active mirror alignment systems have achieved angular stability of mirrors to within $0.1\mu\text{rad}$. The common method is to reflect a separate laser beam off a mirror and onto a photo-sensitive position detector, and employ a feedback circuit to control the mirror with piezoelectric drivers. It is not yet known if the $0.1\mu\text{rad}$ level of stability is achievable in a much more complex and shipboard environment.

A model theory for controlling the vibrations of a single-degree-of-freedom system was developed. The theory was then tested through experiments with a simple active mirror alignment system. Based on the theory, we designed a proportional-derivative (PD) control circuit to provide the negative feedback control loop for our system. Results of the experimental alignment system achieved a reduction of an impressed vibration amplitude by a factor of 5. This is to be compared with sophisticated control circuits at major laboratories, which achieve roughly a factor of 15. In our experiment, the proportional control was nearly the entire cause of this reduction; the derivative control had very little effect.

Although we achieved a significant reduction in system response, further increase of the feedback gain caused an instability to occur at a definite frequency, and the system self-oscillated. This result contradicts our model theory, which predicts that arbitrarily high gains can be used. Preliminary investigations into the cause of this instability suggest that the presence of a number of modes of the mirror mount causes a phase shift that is sufficient for positive feedback to occur.

B. FUTURE WORK

The knowledge gained from these experiments forms a basis for follow-on research towards the development of a prototype active mirror alignment system for a shipboard free electron laser. Continued investigation into the cause of the phase shift should be conducted in order to understand the source of the instability and stabilize the system for continued testing and refinement of the model theory. An understanding of the cause of the phase shift will almost certainly lead to modifications of the control such that a greater gain of the feedback can be applied without the system becoming unstable. A greater gain of the feedback will in turn further reduce the vibrations.

Another possibility is to build or modify a mirror mount so that it is approximately modeled by the single-degree-of-freedom theory. The modification of the mirror mount may involve the use of additional supports to substantially increase the resonance frequencies of the modes other than the main flexural mode. If the modification does not allow a sufficiently high feedback gain, then a control method that involves several degrees of freedom should be developed.

Implementation of a full PID control circuit should also be investigated to continue improving system response. Refinement of the control circuit may also include an appropriate use of notch filters to reduce the effect that mirror mount resonances have on the control circuit. Additionally, an investigation into more sophisticated system components, beyond those used in the experimental alignment system, should be conducted to identify possible components for the prototype shipboard system.

Finally, to move towards the development of a prototype alignment system, the shipboard environment must be characterized to determine the vibrations which the active alignment system will need to suppress.

LIST OF REFERENCES

Advanced Light Source, Lawrence Berkeley National Laboratory, "About the ALS." [<http://www.als.lbl.gov>]. (October 2002)

Behre, C. P. Jr., *Optical Cavity Mirror Stabilization*, Bachelor's Thesis, Old Dominion University, April 2002.

Canon, SLR Camera Systems [<http://www.canon.com/eos/af-tech.htm>]. (October 2002)

Colson, W. B., Todd, A., and Neil, G. R., "A High Power Free Electron Laser Using a Short Rayleigh Length," paper presented at the FEL 2001 Conference, Darmstadt, Germany, August 2001.

Colson, W. B., Naval Postgraduate School, May 2002 (private communication).

Colson, W. B., Naval Postgraduate School, December 2002 (private communication).

Crooker, P. P., Campbell, T., Ossenfort, W., Miller, S., Blau, J., Colson, W., "A Study of the Stability of a High-Power Free Electron Laser Utilizing a Short Rayleigh Length," paper presented at the FEL 2002 Conference, Argonne, IL, September 2002.

Department of the Navy, . . . *From the Sea: Preparing the Naval Service for the 21st Century*, Washington, D.C., U.S. Navy Department. 1992. [<http://www.chinfo.navy.mil/navpalib/policy/fromsea/fromsea.txt>]. (October 2002)

Fowles, G. R., and Cassidy, G. L., *Analytical Mechanics*, 6th ed., Harcourt, Inc., 1999.

Freund, H. P. and Antonsen, T. M., *Principles of Free-Electron Lasers*, pp 1-5, Chapman and Hall, London SE1 8HN, UK, 1996.

Ishihara, N., Iwata, S., Matsui, T., Matsumoto, H., Mizuno, H., Takeda, S., Takeuchi, Y., Yoshioka, M., "A Test Facility of Active Alignment System at KEK," *Proceedings of the 1st International Workshop on Accelerator Alignment*, Stanford Linear Accelerator Center, 1989.

Jackson, J., TRW Aerospace and Defense Group (Airborne Laser), November 2002 (private communication, joe.jackson@trw.com)

JLab, "Free-Electron Laser Description." [<http://www.jlab.org/FEL/>].
(October 2002)

Madey, J. M. J., "The Duke FEL Light Source Facility," *Proceedings of the 1997 Particle Accelerator Conference*, v. 1, pp 24-28, May 1997.

McCarthy, W. J., "Directed Energy Weapons: Implications for Naval Warfare," Occasional Paper No. 10, Center for Strategy and Technology, Air War College, Air University, Maxwell Air Force Base, Alabama. May 2000.

McKinney, W. R., Martin, M. C., Chin, M., Portman, G., Melczer, M. E., Watson, J. A., "Active Feedback Mirror Stabilization System for the IR Beamline 1.4.x Complex," *Advanced Light Source Compendium, 1999*. [<http://alspubs.lbl.gov/AbstractManager/uploads/99034.pdf>].
(October 2002)

McKinney, W. R., Martin, M. C., Chin, M., Portman, G., Melczer, M. E., Watson, J. A., "4-Axis Implementation of the Active Feedback Mirror System for the IR Beamline 1.4.3," *Advanced Light Source Compendium, 2000*. [<http://alspubs.lbl.gov/AbstractManager/uploads/00123.pdf>].
(October 2002)

Pacific Silicon Sensor, Inc., "QP50-6SD Data Sheet."
[<http://www.pacific-sensor.com/pdf/QP506SD.pdf>]. (October 2002)

Pinayev, I. V., Emamian, M., Litvinenko, V. N., Park, S. H., Wu, Y., "System for the Control and Stabilization of OK-4/Duke FEL Optical Cavity," *AIP Conference Proceedings*, v. 451, pp 545-551, December 1998.

Pinayev, I. V., Detweiler, G., Emamian, M., Hower, N., Johnson, M., Litvinenko, V. N., Oakley, O., Park, S. H., Patterson, J., Swift, G., Wu, Y., "Critical Systems for High Peak Power Storage Ring FEL," *Proceedings of the 1999 Particle Accelerator Conference*, v. 4, pp 2468-2470, April 1999.

Shemwell, D. M., Robinson, K. E., Gellert, R. I., Quimby, D. C., Ross, J., Slater, J. M., Vetter, A. A., Zumdieck, J., "Optical Cavities for Visible Free Electron Laser Experiments," *Nuclear Instruments and Methods in Physics Research*, v. A259, pp 56-61, 1987.

Shinn, M., "Engineering Design for the Upgrade FEL Optical Cavity," JLab Technical Note 02-013, 22 April 2002.

Siegman, A. E., *Lasers*, pp 663-769, University Science Books, 1986.

Svelto, O., *Principles of Lasers*, pp 452-454 Plenum Press, New York, 1998.

Todd, A. M., "Workshop on Free-Electron Laser Development for Naval Applications," June 2001. [<http://www.aesys.net/FELworkshop.html>]. (August 2002)

Todd, A.M., Colson, W. B., Neil, G. R., "Megawatt-Class Free Electron Laser Concept for Shipboard Self-Defense," *SPIE Proceedings*, v. 2988, pp 176-184, February 1997.

University of Maryland, Institute for Research in Electronics and Applied Physics, "What is a Free Electron Laser."
[<http://www.ireap.umd.edu/FEL/whatis.htm>]. (October 2002)

THIS PAGE INTENTIONALLY LEFT BLANK

BIBLIOGRAPHY

Anderson, E. J., *Total Ship Integration of a Free Electron Laser*, Master's Thesis, Naval Postgraduate School, Monterey, California, September 1996.

Fuller, C. R., Elliot, S. J., and Nelson, P. A., *Active Control of Vibration*, Academic Press, 1996.

Kienholz, D. A., "Active Alignment and Vibration Control System for Large Airborne Optical System," paper presented at the SPIE Smart Structures and Materials Conference, San Diego, CA, March 2000

McDonald, A. C., and Lowe, H., *Feedback and Control Systems*, Reston Pub. Co., 1981.

McGinnis, R. D., *Free Electron Laser Development for Directed Energy*, Ph. D Dissertation, Naval Postgraduate School, Monterey, California, December 2000.

Ogata, K., *System Dynamics*, 3rd ed., Prentice Hall, 1998.

THIS PAGE INTENTIONALLY LEFT BLANK

INITIAL DISTRIBUTION LIST

Defense Technical Information Center
Ft. Belvoir, VA

Dudley Knox Library Naval Postgraduate School
Monterey, CA

Physics Department
Naval Postgraduate School
Monterey, CA

Professor Bruce Denardo
Naval Postgraduate School
Monterey, CA

Professor Thomas Hofler
Naval Postgraduate School
Monterey, CA